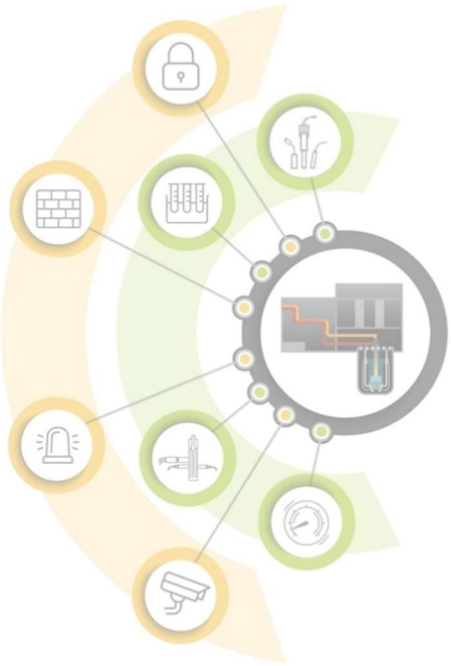

Advanced Reactor Safeguards

Material Control and Accounting Regulatory and Technical Considerations for Microreactors

Final Report Prepared for
US Department of Energy

Robert Weinmann-Smith[1], Athena Sagadevan[1], Christopher Morris[1], Elena Guardincerri[1], Matthew Carpenter[1], Amanda Gehring[1], Holly Trellue[1], Vedant Mehta[1], Michael Browne[1]

[1]Los Alamos National Laboratory

December 2021
LA-UR-22-21265

Los Alamos NATIONAL LABORATORY

ABSTRACT

New microreactors must comply with the Material Control and Accounting (MC&A) regulations in 10CFR74. The objective of MC&A is to verify that the nuclear material is not stolen or diverted to unauthorized users. Microreactors have unique features which pose new challenges to addressing these regulations. This work considers general approaches and methods for microreactor MC&A based on the reactor life cycles which have been proposed by microreactor vendors.

One key aspect of MC&A is measurement of the nuclear material. Measurement of microreactor fuel could be especially important because the cores may be sealed for up to 20 years, preventing direct visual confirmation. Measurements could also be especially challenging due to the thick shielding designed around microreactors. This work evaluates a range of techniques used in medical, industrial, and nuclear fields. The cost, time, and performance of the techniques were estimated. Finally, for a promising technique of using in-core neutron detectors, the feasibility was analyzed in detail.

ACKNOWLEDGEMENTS

This work was funded through the Advanced Reactor Safeguards Program, Office of Nuclear Energy within the United States Department of Energy.

CONTENTS

LIST OF FIGURES

ACRONYMS AND DEFINITIONS

Abbreviation	Definition
2D	two-dimensional
ARDP	Advanced Reactor Demonstration Program
ARS	Advanced Reactor Safeguards
CCD	Charge coupled device
CFR	Code of Federal Regulations

Abbreviation	Definition
cps	counts per second
DSIC	Decision Sciences Corporation
DT	Deuterium-Tritium
INL	Idaho National Laboratory
ITAAC	Inspections, Tests, Analyses, and Acceptance Criteria
kg	kilogram
km	kilometer
LANL	Los Alamos National Laboratory
lbs	pounds
LWR	Light Water Reactor
MARVEL	Microreactor Applications Research Validation and Evaluation
MBA	Material Balance Area
MC&A	Material Control and Accounting
MCNP	Monte Carlo N-Particle
MeV	Mega electron volt
mm	millimeter
MW	Megawatt
n/s	neutrons per second
NCR	Nuclear critical assembly reactor
NDA	Non Destructive Assay
NIST	National Institute of Standards and Technology
NRC	Nuclear Regulatory Commission
SNM	Special Nuclear Material
U	uranium
UNCL	uranium neutron coincidence collar
UO2	uranium dioxide
US	United States

1. INTRODUCTION

The US DOE-NE's Advanced Reactor Demonstration Program was launched to demonstrate a variety of advanced reactor designs. The Advanced Reactor Safeguards sub-program is tasked with supporting near term research in areas related to materials accountancy and physical protection to help facilitate the deployment by vendors. Reactor deployment is regulated by the Nuclear Regulatory Commission (NRC). One aspect of these regulations is Material Control and Accounting (MC&A). The objective of MC&A is to verify that the nuclear material is not stolen or diverted to unauthorized users. For advanced reactors, it is unclear how to satisfy the MC&A regulatory requirements because unique features of the reactors pose new challenges and questions which have not previously been addressed. Such challenges are especially true for microreactors. This work addresses the value of measurement based quantification of the nuclear material, and identifies technical approaches for such quantification. This final report has some overlap with the project's Phase 1 report. All chapters have been revised and Chapter 6, detailed calculations of in-core neutron detectors, is entirely new.

Microreactors are small reactors with a thermal power level of about 10KW to 10MW. They would be used for small remote power needs such as remote villages, industrial operations, or military sites. They could be fabricated and sealed at a factory, transported on a truck, and operated at the site. They could be operated for as long as 20 years before being refueled or disposed, and would require much less maintenance and operating staff than traditional reactors. Microreactor proposals have included a broad range of technical designs and operating life cycles.

MC&A is generally performed by tracking the nuclear material in a formal accounting system. The regulations are described in 10CFR74. The material input into the system should equal the material currently in the system and the material that has left the system. If this material accounting balances then the material has not been diverted, and an unbalanced accounting provides timely detection of diversion. Determining the material content at the various stages is performed through a variety of techniques ranging from simple methods such as counting the number of items to complex calculations or radiation measurements to determine the amount of material.

Microreactors add unsolved challenges to the traditional methods of MC&A. First, the regulations applied to microreactors will dictate the MC&A requirements. The regulations were written for traditional LWRs. The NRC is in the process of writing regulations for advanced reactors as a long-term solution which is described in more detail in Appendix A. In the short term the NRC will consider vendor submissions under the current LWR process, but they expect significant use of the exemption process. One of the most important conclusions of this work, explained in Chapter 2, the MC&A requirement can be satisfied by item counting regardless of the microreactor's unique features. Other differences in MC&A approaches for microreactors are identified in Chapter 3.

However, while not currently required to satisfy 10CFR74, the proposed life cycles make it far more likely that circumstances would call for assay of the fuel without opening the reactor. Microreactors' frequent transportation, operation in remote areas, and limited onsite staff and capabilities, may result in scenarios unusual for LWRs which would benefit from direct verification of the presence of the nuclear material. The long term sealed cores would prevent visual inspection of the fuel rods or elements themselves. Also, such measurements are very likely to be required for International Safeguards, which is of interest to US reactor developers accessing international markets. Development of this capability now through safeguards by design integration will enable more effective and efficient methods. The concerns identified by an assumed life cycle framework are discussed in Chapter 3.

Should the need arise to assay the nuclear fuel inside a sealed core, the technical challenges to do so are significant. Microreactors have thick neutron and gamma shielding to allow their operation above or just below grade with no or minimal containment buildings. They will be sealed for decades and are not designed for frequent access and refueling like traditional LWRs. The use of traditional radiation measurements may not be feasible due to this shielding. A similar challenge is the assay of fuel in dry storage casks. The quantity of fuel and the amount of shielding is similar to microreactors. Methods to perform this assay have been investigated for three decades and a single best solution has still not been identified. These methods are reviewed in Appendix C. Developing a solution for microreactors while they are still under design by vendors could avoid this costly issue, especially if the solution could be incorporated underneath the shielding.

This work broadly evaluated a range of assay techniques for their feasibility in Chapter 5. To ensure a thorough review, application of similar techniques in industrial and medical fields is described in Appendix B. The technical solutions range from low cost approaches which use the microreactor's existing systems to expensive methods which are entirely independent of and external to the microreactor. The feasibility, performance, and cost of the techniques are discussed in this paper and require further evaluation. The technical approaches include visual inspection, weight measurement, measurements of the radiation emitted by the fuel with the microreactor's own instrumentation and with external instrumentation, and radiography measurements. Radiography is the measurement of radiation passed through an object to determine the object's characteristics. The most common application is medical x-rays. Radiography generates an image of the internals of the object. Radiography of a microreactor will be challenging due to the large amount of shielding which may prevent a clear image. Still, the measurement could be designed to confirm the presence of the fuel.

The most promising technique was using in-core neutron instrumentation to passively measure the neutron emissions from the fuel. This technique would be inexpensive, and could either use operator instrumentation or be added specifically for this purpose. The technical feasibility of the technique was calculated in detail to estimate its performance in Chapter 6. The evaluation assumed fresh fuel only but the same concept is likely feasible for a spent core. This evaluation suggested the technique's performance would be quite good. A more detailed evaluation using commercial reactor designs and optimized for vendor concerns would be a valuable next step.

2. MC&A REQUIREMENTS OF NUCLEAR POWER PLANTS

There are multiple reactor licensing paths which have different requirements and dictate which regulations are applicable. Currently microreactor licensing will be done under the traditional methods such as 10CFR50 and 10CFR52. The exception process will be used for aspects which are not applicable to microreactors. Reactors are divided into power reactors and non-power reactors such as research and test reactors. The distinction is because non-power reactor nuclear material and spent fuel inventories are lower than in commercial power reactors, so the risk to the public is lower and requirements fewer than for a power reactor. Note that when it is complete, microreactor licensing will occur under advanced reactor regulations, which are expected to be finalized in late 2024 and labeled 10CFR53 (see Appendix A for more details). Microreactor vendors argue their spent fuel inventory is low so 10CFR50 also applies to them. The NRC will need to decide the regulation path. In this paper we assume that material control and accounting requirements will match those of a commercial power reactor. This assumption will allow us to address the most challenging case and strictest requirements if necessary. If lesser requirements are decided either through the power reactor regulations with exemptions or the non-power reactor regulations, then the path to successful reactor deployment is even easier.

Material control and accounting requirements of nuclear power plants are specified in 10CFR74, Material Control and Accounting of Special Nuclear Material [1]. The requirements related to nuclear power plants are found in Subpart B, General Reporting and Recordkeeping Requirements. Power reactors are considered utilization facilities because they use nuclear fuel. They do not typically fall under requirements in Subparts C, D, and E, for low, moderate, and strategic special nuclear material.

Within Subpart B, regulations applicable to MC&A for power reactors are 10CFR74.11, 74.13, 74.15, and 74.19, which is all of the regulations in Subpart B except 74.17 which describes reporting related to Subparts C, D, and E. Regulation 74.11 requires reporting within 1 hour of discovery of any loss or theft or unlawful diversion of SNM. Regulation 74.13 requires the submission of complete Material Balance Reports, concerning SNM that has been received, possessed, and transferred, among other requirements. It must also include a Physical Inventory Listing Report. Regulation 74.15 requires Nuclear Material Transaction Reports concerning transfers, receipts, or shipments of SNM. Regulation 74.19 requires the keeping of records showing the receipt, inventory (including location and unique identity), acquisition, transfer, and disposal of all SNM, for periods of years or sometimes indefinitely. It also requires the licensee to establish, maintain, and follow written MC&A procedures sufficient to account for all SNM in possession. A physical inventory of all SNM shall be conducted at least every 12 months.

These regulations form the overall requirements, but their level of detail is quite general. Additional detail can be found in the regulatory guides which describe specific methods of how the regulations may be satisfactorily addressed. Regulatory Guide 5.29, Special Nuclear Material Control and Accounting Systems for Nuclear Power Plants, and its subsequent references contain more detail. The guide states that it applies to all nuclear power plants, so it does apply to microreactors. It also states that different methods will be deemed acceptable if they provide an acceptable basis for licensing. Alternative solutions to achieve the same MC&A capabilities and address the requirements will be discussed in this report.

Most of the guidance deals with the procedures and organization required. Some guidance is related to controlling the fuel and may be relevant for microreactors. Item control areas (ICAs), similar to Material Balance Areas (MBAs) are required to be designated. Receiving and shipping, internal transfer, and physical inventory of SNM is required. Characterization and identification of SNM, including element and isotopic calculations, should be addressed.

Fuel assemblies are considered individual items. Items are identified by unique identifiers, and the physical inventory method is an item count. This specifically means the SNM within the fuel assembly does not need to be measured via nondestructive assay (NDA) techniques for MC&A purposes. The one exception is if the fuel becomes separated from a fuel rod, then the amount of SNM should be estimated with methods that may include NDA measurement.

Most importantly, reactors are considered one item for inventory purposes, and may be verified by item counting. Reactors do not need to be opened to verify the assemblies inside and NDA techniques are not required to measure the SNM without opening the reactor. The fuel assembly unique identifiers are verified upon loading before the core is sealed. Thus direct measurement of the fuel is not an MC&A requirement to satisfy 10CFR74. Still, such measurements may be valuable for other purposes.

3. MICROREACTOR LIFE CYCLE FRAMEWORK

This work assumes a representative microreactor life cycle framework and a representative specific microreactor design in order to evaluate potential measurement scenarios and technology solutions. The assumed life cycle and microreactor are not based on a specific vendor design but the key features are characteristic of most microreactors. There may be some small differences in a specific life cycle or reactor design, but the concepts in this work can be readily translated to any design. There is some uncertainty which life cycles and designs are realistic. Multiple life cycle concepts have been proposed. The selected vendor designs and capabilities are given in Table 3-1 [2-15]. Since no microreactor has ever been licensed, built, or operated through a full life cycle, real-world implementation may differ from these proposals.

Table 3-1. Selected commercial microreactor characteristics

Reactor	Type	Full power core lifetime	Transportable?	Installation timeline	Location of fuel loading	Refueling planned?
Westinghouse's eVinci	Heatpipe thermal neutron	3+ years	Yes	<30 days	Factory	Yes
Oklo's Aurora	Heatpipe fast neutron	20 years	No	N/A	On-site	N/A
BWXT's Advanced Nuclear Reactor (BANR)	High temperature gas cooled	N/A	Yes	N/A	N/A	N/A
X-energy's Xe-Mobile	High temperature gas cooled	3+ years	Yes	7 days	N/A	N/A
Urenco's U-Battery	High temperature gas cooled	5 years	No	N/A	N/A	Yes
Radiant's Kaleidos Fission Battery	High temperature gas cooled	4-8 years	Yes	72 hours to install, removal after 1 week of shutdown	Factory	N/A
Ultra Safe's MMR-5/-10	High temperature gas cooled	20 years	Yes	Months	Factory	Fuel cartridge replaced if needed after 20 years
Holos' HolosQuad	High temperature gas cooled	3-20 years	Yes	N/A	Factory cartridge	Yes

The assumed life cycle framework used in this work includes the major phases which a microreactor is expected to undertake. First the microreactor is fabricated at a factory where the core and shielding is sealed with the fuel inside. The reactor is transported by truck to the operation site

where it is stored for some time in preparation for installation and operation. The microreactor is operated at the site for a period of time which could be as much as 20 years, but possibly much shorter. Then uninstallation, transportation to a disposal site, and eventual disposal occurs. It is also possible the reactor could be refueled and redeployed, but for our purposes that scenario is identical to the first transportation and operation so it is excluded. The life cycle is depicted in Figure 2-1.

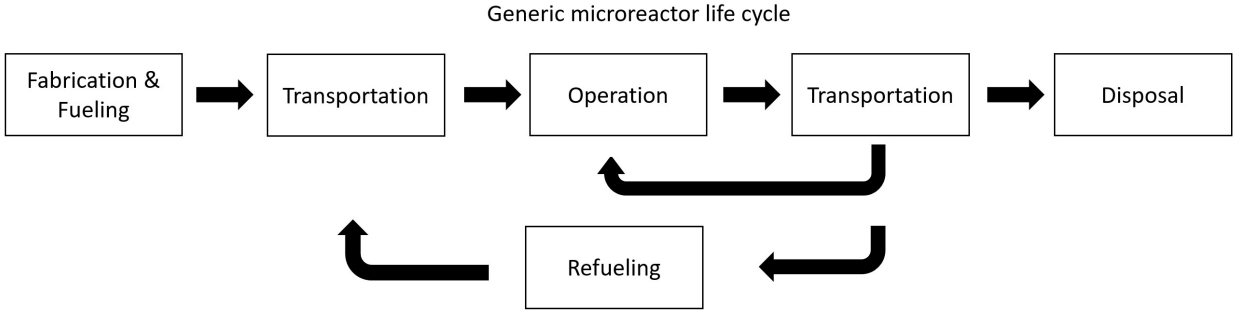

Figure 2-1. Life cycle of a microreactor.

3.1. Fabrication and fueling

The microreactor would likely be built at a factory, fully assembled and sealed, and then shipped to the deployment site. Alternatively, if it is fabricated at the operation site, it would at some point be sealed. After the system is sealed, inspections become more limited.

The first regulatory issue is that the regulations consider the fundamental fuel unit to be a fuel assembly. MC&A is performed by item counting at the assembly level. This makes sense for LWRs because an assembly is a fixed, sealed structure containing fuel and is the smallest typical fuel unit at a LWR. For microreactors the fundamental fuel unit is mostly likely a fuel pin or rod, although this may depend on the microreactor design. The equivalent treatment would then be for rods to have individual unique identification numbers and for the rods to be tracked at the item level once they are created at the fuel fabrication facility. Then the microreactor fabrication facility would likely satisfy the MC&A requirements with item counting as described in Regulatory Guide 5.29. Note some NDA capability may be required to address fuel separated from a fuel rod in the event of fuel damage. The fabrication facility's item control area structure would likely resemble a LWR site, having receiving, fuel storage, and reactor areas in common.

This approach may introduce a significant difference in the number of items to be tracked because a LWR core has hundreds of fuel assemblies while a microreactor may have thousands of fuel rods. However the total tracking effort would be significantly reduced because the microreactor core would only be loaded once and then treated as a single item, limiting the tracking effort to the fuel fabrication and microreactor fabrication facilities. In contrast, a LWR reloads its core about every 1.5 years, shuffling assemblies between fresh fuel storage, the reactor, and spent fuel storage, which in comparison is a large tracking effort. LWRs also receive about 50 fresh fuel assemblies for each core reload. After decades of operation this accumulation may reach over 1,000 assemblies.

At the factory the fuel rods would be assembled into the microreactor. Once the microreactor is sealed, it may be considered either a container or a reactor per the regulatory guide, both of which are treated as a single item. If the microreactor is considered a reactor then the location and unique identification number of each rod must be verified, and then the reactor is treated as a single item. However this consideration is less applicable from a MC&A and safeguards and security perspective

because the reactor will not be operating nor will it contain spent fuel and so it is not self-protecting. Another difference is that a fully constructed sealed microreactor could remain in storage for extended periods of time for various reasons. The storage time may be much longer than the typical 1.5 years LWR reactors stay sealed for. At this stage it may be more accurate to consider the microreactor as a sealed container. The fuel inside would need to be inventoried before sealing with a tamper-safing device to be counted as a single item. The tamper-safing device provides higher confidence that the fuel rods in the reactor are present. Such a device may also be required for shipping as described in Regulatory Guide 5.29. Alternatively, the reactor core could be left open periodically or consistently to inventory the rods individually as items.

The reactor fabrication facility also has safety and security concerns. In the traditional method where reactors are built at the operation site the vendor and the NRC can both perform inspections. While the microreactor can be inspected at its construction facility, once the container is sealed it will be difficult or impossible to inspect many of the reactor's systems. Specifically, the fuel, heat transfer mechanisms, the control drums, and much of the containment wall will be fully sealed into the core. Heat exchangers and control rod systems will remain near the core and probably will not be shielded well enough to allow safe access by a person once the reactor has been operated. In a LWR these systems are much more accessible for inspection. This work is primarily focused on verifying the presence of the nuclear material, but some radiography techniques identified in this work may be valuable for safety inspections.

Overall, the microreactor fuel rods or reactor core are readily inventoried under item counting and the systems are readily available for inspection, so there are likely no barriers to satisfying the regulations at this stage.

3.2. Transportation and Site Storage

Once the microreactor is sealed, it will be transported to the operation site where it will be stored in preparation for installation. This process departs from traditional LWR methods where only the fuel is transported to the operation site and the rest of the reactor is constructed in place. The regulatory guide on MC&A for nuclear power plants considers the reactor operator (the 'utility'), the shipper, and the shipping vendor, as separate entities. The microreactor operator may be two or all three of these entities and have their roles and responsibilities. Given the smaller reactor size, one proposed operating model is a vendor or utility operating a fleet of reactors remotely from a central location. Note the considerations of a microreactor as a sealed container or reactor in the previous section are only applicable as internal controls. Shipping may have additional requirements.

The receipt of SNM requires a reconciliation of the quantity and identification of items between shipper and the utility. For LWR fuel assemblies, the packaging can easily be opened and the assemblies inspected by item counting as specified in the regulatory guide to confirm the material arrived and provide an 'input' value into the material accounting system. If more thorough measures are needed, for example to resolve discrepancies, NDA methods are feasible because the assemblies are readily accessed with minimal shielding (the fuel clad) between the NDA equipment and the SNM itself. In contrast, a sealed microreactor core does not allow item counting of the fuel rods within. It also has significant shielding which prevents traditional NDA methods from being employed. If the sealed microreactor is not treated as a single item during shipping and receiving, or if it cannot be opened easily at the receiving site, then alternative approaches must be used. NDA

techniques identified in this paper may satisfy this need by confirming the presence of the nuclear material for item receipt and for discrepancy resolution.

If the microreactor must be measured in some way before the reactor goes into operation, some aspects of this stage of the fuel cycle may assist in performing this measurement. Since the microreactor will be shipped on a truck, it is already mobile and can be moved into position for a measurement. It is also lifted off the ground which may allow access underneath the reactor, depending on the measurement type. The construction equipment on site for installation, perhaps a crane or equipment preparing the below-grade area, could be used to lift the reactor or move it, hold the inspection equipment, or assist in removing or installing some of the shielding.

Once the microreactor has been satisfactorily received by the utility, the MC&A approaches for internal control specified in the regulatory guide and described in Chapter 2 may again apply. Namely, the microreactor and fuel rods within may be treated as a single item for inventory purposes.

In addition to MC&A considerations, there are safety concerns which may be relevant at this stage in the life cycle. Inspections, Tests, Analyses, and Acceptance Criteria (ITAACs) are required by 10CFR52 to be performed by the operator and reviewed by the NRC prior to operation. These tests are identified by the NRC as part of the licensing process. Their purpose is to 'provide reasonable assurance that the facility has been constructed and will operate in conformity with the license, the provisions of the Act, and the Commission's rules and regulations' [10CFR52.97(b)][16]. Some ITAACs can be performed at the factory during fabrication. Additional ITAACs may be required after transportation or installation at the site, to address potential issues which may have occurred at either step. Some systems which are sealed into the core may be impossible to inspect directly. Radiography may provide inspection of these systems, and NDA measurement of the fuel may also be valuable for safe startup.

3.3. Operation

Microreactors have unique operating characteristics compared to traditional LWRs. LWRs are refueled about every 1.5 years, which allows access for visual inspection and inventory of the fuel assemblies. During the 1.5 years of operation the reactor is sealed and is considered a single item for inventory. The regulations do not provide further discussion regarding the duration, but this may be considered temporary or acceptable on a 1.5 year time scale. A microreactor may operate (either continuous or intermittent full power) for 20 years or more without refueling, causing the fuel to go 10x longer without direct visual inventory. NDA based fuel measurements could improve the frequency of direct inventory. In fact, if direct inventory is required at any time, fuel measurements may be the only option because it may not be possible to open the reactor on-site due to the significant industrial capability required to deal with shielding the radiation once the reactor has been operated.

MC&A and inventories are only one aspect of safeguard's goal of securing the nuclear material. Because a microreactor has less nuclear material, it will likely have less safeguards protections (guards, gates, etc.) to achieve the same risk as a LWR. The combination of significantly delayed direct fuel inventories and reduced protections may cause an unacceptably high increase in risk. A fuel measurement could serve as a direct inventory without interrupting operations by opening the reactor. When considering the comprehensive safeguards approach, a fuel measurement could

economically increase the frequency of direct inventories, allowing for a reduction in other safeguards requirements.

The approach to measuring the fuel depends on the specific operating status of the microreactor. If the microreactor is at full power then neutronic characteristics likely serve as a measurement of the fuel. For example, the control rod position for criticality, or the neutron flux profile from in-core instrumentation demonstrate that the fuel is present because if it was absent the core would have different characteristics. If the reactor operates continuously for 20 years this data could act as a continuous confirmation of the presence of the nuclear fuel. Also the high radiation environment would add additional protection. If the reactor shuts down occasionally with minimal downtime then the neutronic characteristics confirm the presence of the fuel before and after the shutdown. If the shut down is extended, or if there is some other motivation to use them, one of the other techniques discussed in this report can be used to measure the fuel.

Finally, from a safety point of view, the expansiveness of a LWR facility allows access to many of the systems most of the time for safety related inspections. The compact sealed design of microreactors will likely prevent most of these inspections due to access and radiation health safety issues. Some of the radiography technology which could measure the fuel directly could also be used to image the other microreactor systems as a safety inspection.

3.4. Transportation and Disposal

At the end of the reactor's operating life, it will likely be transported to a disposal site. In the US, spent nuclear fuel at traditional LWRs remains on site to be stored safely and securely. Since a microreactor will be deployed to remote areas with little infrastructure, it will likely be returned to a central storage location for long term disposal. Currently, no storage or disposal method exists, which is a major concern that will need to be addressed in the future. Often in the nuclear industry, if disposal were to occur, there are still likely delays for years or decades where the fuel would need to be stored before disposal. If disposal is not possible the fuel may be stored indefinitely. Confirming the status of the nuclear fuel would be a major requirement which could be addressed by the techniques described in this report. Most of the measurement techniques could be repeated at regular intervals and function as well on day 1 as they do on year 100. Other techniques such as using the reactor's in-core instrumentation will require some of the reactor's systems to remain operational. Radiation measurements may need to account for radioactive decay and be benchmarked to some initial measurement. Confirming the fuel would be a major step towards addressing the long-term storage or disposal needs.

4. OPPORTUNITIES FOR SAFEGUARDS BY DESIGN

Safeguards by design involves analyzing methods and adjusting reactor design to make nuclear material accounting far easier. The term is typically applied to international nuclear safeguards but translates to domestic MC&A as well. Since microreactors are early in the design phase, it is an excellent time to incorporate such adjustments.

When considering these changes, it is important to also consider the burden and cost added to the vendor in fabricating and operating the reactor. By considering MC&A early in the design process, the solution should be cheaper and more effective than implementing a solution afterwards.

One possibility is to perform measurements of the fuel underneath the core shielding. One of the most valuable nuclear material accounting measurement methods is measuring the radiation emitted by the fuel, but the large amount of shielding around the core makes that extremely difficult. If the measurement equipment could be incorporated underneath the shielding then a much better measurement could be performed, but further specific details must be considered. This measurement equipment may be damaged by the large amount of radiation during operation. Perhaps one set of equipment could measure the emission of gamma and neutron radiation from the fresh fuel and be removed or left in place to be destroyed once the reactor is operated. A second set of robust equipment could perform the measurements of the spent fuel during and after operation. The equipment could move within the reactor to areas of lower radiation while the reactor is on, or it could be behind some of the core shielding but not all of it.

Another option is to assemble the shielding on site. If the microreactor and its fresh fuel, which emits very little radiation, was shipped without the core shielding and was assembled on site, it would give an opportunity to measure the fresh fuel upon arrival at the site before the shielding is installed. This option may address the most vulnerable fuel cycle phase, as once the core is sealed and not moved there is added confidence and safety that the material is intact. The additional burden of this process may be lower than expected. The microreactor would still need to be shipped safely in a robust shipping container, but the core shielding is designed to reduce dose to nearby people during operation, not to survive a crash and the other various requirements of transporting fresh fuel. A transportation container would already be required to protect the fuel. If the reactor must be shipped inside the shielding, being able to temporarily remove the shielding at the installation site serves the same purpose.

Finally, the reactor's own neutron instrumentation could be used to perform the MC&A measurements. This is likely possible without any changes to the current instrumentation, with some degree of efficacy. Understanding the application of neutron instrumentation to MC&A was performed in Chapter 6. A reactor's specific instrumentation may be adjusted to improve its MC&A performance, which would be safeguards by design.

5. SUMMARY OF RADIATION MEASUREMENT AND RADIOGRAPHY TECHNIQUES

First, we describe the technical details of the assumed design basis microreactor and the relevant fundamental radiation characteristics to inform why a specific technique may be preferable. Then we organize the description of measurement techniques into external active interrogation techniques and passive techniques. The techniques were evaluated for their cost, measurement time, and performance. A summary of the results is included in Table 5-3. In-core neutron measurements were identified as particularly advantageous due to their low equipment cost and high performance. Their technical feasibility is evaluated in detail in Chapter 6.

As a summary of the technical considerations, the external techniques utilize radiation which originates from outside the microreactor. This radiation is independent from the state of the microreactor and thus these techniques will be functional at any stage of the reactor's life cycle. The downside is that, for X-ray and neutron techniques, the external radiation must be generated with equipment that adds complexity and cost to the technique. Depending on the technique, they may also be less sensitive if the fuel was replaced with a material like steel. Passive techniques measure the radiation emitted from the fuel. When the fuel is fresh, before the reactor has been operated, the emission is low but may be sufficient radiation for measurement. Reactor operation creates fission products in the fuel which generate 1,000 to 1,000,000 times more radiation and will require different equipment to measure. These techniques need to be calibrated to fuel burnup or benchmarked to an initial measurement. This method of calibration adds complexity and uncertainty.

5.1. Microreactor Characteristics and Radiation Properties

Multiple microreactor concepts have been developed, but none have been deployed yet. In this report a non-commercial design, the Los Alamos National Laboratory (LANL) MegaPower reactor, is studied as the design basis microreactor because its technical details are widely available and, for the purpose of radiation measurements and radiography, its features are sufficiently similar to other commercial designs. MegaPower's basic characteristics are [17]:

- 5 Megawatt (MW) thermal, about 2 MW electric, 5 year full power lifetime
- Cooled by 1,224 liquid metal potassium (K) heat pipes at 675°C
- Hexagonal stainless steel monolith to contain UO_2 pins and heat pipes
- Fast neutron spectrum, no water in the core
- 5.22 metric tons of UO_2 fuel in 2,112 fuel pins, 19.75% enriched
- No moving parts, valves, pumps, or high-pressure systems

Figure 5-1 shows a radial cross section of the MegaPower reactor. The middle hexagon is an air gap for the control rod structure which controls criticality along with the outer control drums. The shielding colors and dimensions are shown in Table 5-1. From the table, the most prominent attenuators are the 15.24 cm B4C neutron shield and the 10.16 cm lead gamma shield.

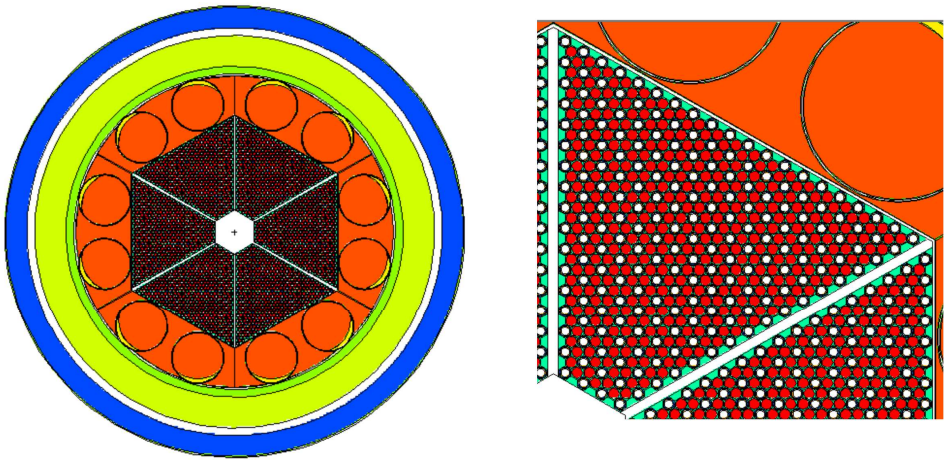

Figure 5-1. Radial cross section of the MegaPower reactor and fuel detail.

Table 5-1. Dimensions of the MegaPower reactor.

LANL MegaPower	Thickness (cm)
Inner stainless steel containment vessel (green)	3.81
B_4C neutron shield (green/yellow)	15.24
Air gap for shield cooling (white)	3.81
Lead gamma shield (blue)	10.16
Outer stainless steel outer wall	0.635

The fundamental radiation transport characteristics were simulated using the MCNP® code [18]. The fraction of neutron and gamma particles which would transmit from one side of the reactor to the other was found. This simple quantity provides understanding of the challenges of performing measurements through the reactor shielding. A 14 MeV neutron or 15 MeV gamma generator was placed on one side of the system, and the fraction of neutrons and gammas detected in an arbitrary volume on the other side of the reactor were tracked. The results are binned according to their energy, which is relevant because various detection instruments have different efficiencies for different energies, and can be optimized for a specific energy. Also, energy can be used to distinguish the radiation above background or to indicate other physics effects, and so the fraction of particles that reach the other side at a specific energy may be useful. The errors are fractional relative errors. They are large for some bins, but the order of magnitude of the results is likely accurate. The results are the flux in particle/cm^2 per starting particle. For example, the result from 1 to 10 MeV is 3E-7, meaning for every one starting particle the flux is 3E-7 n/cm^2. For a neutron generator that produces 10E12 n/s, the flux may be 3E5 n/cm^2/s.

Microreactors are shielded to ensure dose rates on the outside are below regulatory limits. While this is necessary for safety, the shielding greatly increases the difficulty in determining the contents of the microreactor core, which is a MC&A concern.

Table 5-2. Simulated neutron and gamma flux on the opposite side of the microreactor from 14 MeV neutrons and 15 MeV gammas.

Neutrons			*Gammas*		
energy (MeV)	**n/cm^2**	**error**	**energy (MeV)**	**γ/cm^2**	**error**
0.001-0.1	8.4E-09	0.15	0.001-0.1	3.2E-14	0.70
0.01-0.1	6.0E-08	0.04	0.01-0.1	4.0E-12	0.57
0.1-1	4.3E-07	0.02	0.1-1	3.2E-10	0.56
1-10	2.8E-07	0.02	1-10	5.4E-10	0.56
			10-100	1.6E-11	0.67
total	7.8E-07	0.0172	total	8.8E-10	0.56

For active interrogation, a major concern is the cost to generate the particles. Muons are generated naturally which eliminates this aspect of their cost, although it provides a limitation of fixed interrogation flux preventing a technique to improve measurement time. Neutrons, high energy x-rays, and protons can all be generated with various equipment. The overall costs and performance of these techniques will be similar, and identifying the best option between them can be done if active interrogation is determined to be the preferred technique in the future.

5.2. Active Interrogation – External Radiation Techniques

5.2.1. Cosmic ray muon radiography

Muon radiography or tomography could provide high resolution 3D images of the core and fuel of the microreactor which is valuable for MC&A and for safety related inspections. This technology is the most mature of the active interrogation techniques. A muon radiography system consists of one or more pairs of muon trackers with the object of interest placed between them. Muons are sensitive to the atomic number and densities of material so they can be used to distinguish the core and shielding. No active source is required because the interrogating muons are produced naturally in the atmosphere and continuously shower on Earth, greatly reducing the safety requirements compared to radiographic techniques that require active sources.

Muon tomography has been used to image a variety of large industrial objects. An example of a muon radiography system scanning a truck is illustrated in Figure 5-2. A 10 minute reconstruction using LANL algorithms of a tractor trailer with cargo and hidden test objects is shown in Figure 5-3. Each of the test objects was 20 kg of high-z material with dimensions of 10x10x10 cm^3. These systems, manufactured by Decision Sciences International Corporation (DSIC) [19] are currently being deployed at sites around the world for examining cargo for contraband. The deployed systems have a field of view of about 4x20x4 m^3, which could encompass a microreactor.

Figure 5-2. Muon scanner installed by Decision Sciences Corporation in Freeport, Bahamas, examining a tractor trailer.

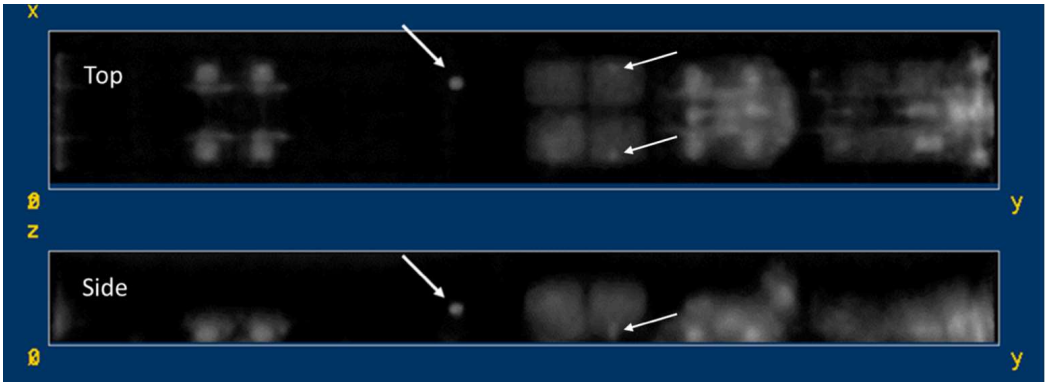

Figure 5-3. Top and side view made with 10 minutes of exposure of a tractor trailer loaded with cargo and 3 mock nuclear threat objects marked by arrows.

Muon tomography has been used to inspect nuclear reactors, including the nuclear critical assembly reactor (NCR) at Toshiba [20] in Japan. The measurement was taken with the LANL built 4x4 foot^2 mini muon tracker (MMT) [21]. The object of interest consisted of a 40 cm diameter cylindrical array of fuel rods with a 20 cm void at the center, plus two individual fuel rods located to the side of the cylinder, in front and behind it. Figure **Error! Reference source not found.**5-4 shows the placement of the two muon trackers relative to the object of interest. Data were collected in this configuration for about 4 weeks but significant results were obtained much faster. The array of rods were visible after 4 hours and the void after 1 day of measurement. Figure 5-5 demonstrates the resolution of the measurement. The figure also shows an accurate Monte Carlo simulation capability which can be used to model application of the technique to microreactors. Three-dimensional images could additionally resolve individual fuel rods located above and behind the main assembly, Figure **Error! Reference source not found.**5-5.

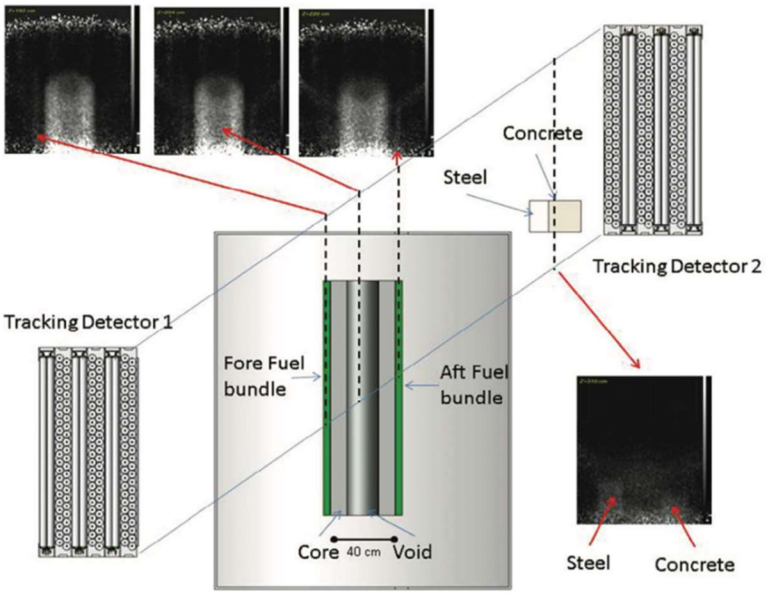

Figure 5-4. Composite drawing showing the layout of the experiment and reconstruction slices showing the individual fuel rod separated from the main assembly.

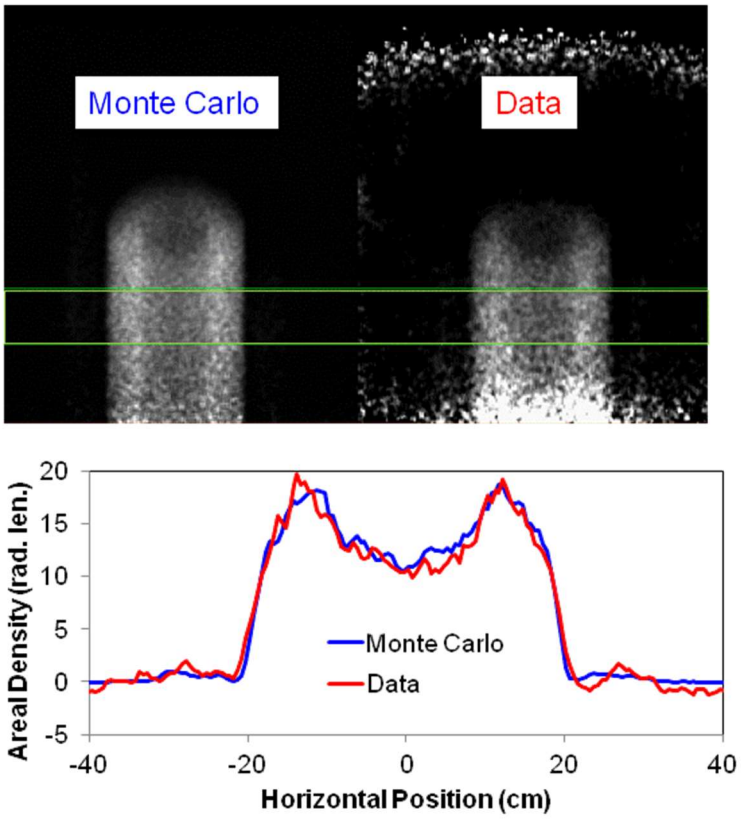

Figure 5-5. Comparison of a Monte Carlo simulation and measured data for images of a fuel assembly.

Other applications include measurements on a Westinghouse MC10 storage cask at Idaho National Laboratory (INL) using the MMT demonstrating the detection of missing fuel bundles with high reliability [22]. These measurements required two weeks of exposure because, due to the detector's small size, it had to be moved through the course of the measurements to obtain full coverage of the fuel cask.

Monte Carlo techniques have been used to test more advanced reconstruction techniques [23]. These demonstrate the sensitivity of muon tomography to a set of diversion scenarios such as the replacement of high burn up fuel assemblies with fresh fuel inside storage casks. Using large, round detectors allow this information to be obtained with about 1 day of exposure.

Figure 5-6 shows how a pair of 12 x 18 ft^2 trackers could be used to image Westinghouse's eVinci reactor, either on a truck bed or installed. Such a configuration could obtain 3D images of the interior of the reactor with a resolution of approximately 10 cm in less than 2 weeks. In some microreactor configurations the reactor is fully or partially underground. If the measurement were inside a 1m deep pit the count time would not increase. The cost of a standard 24 ft x 36 ft DSIC drive through scanner complete with electronics a detector hub, a computer cluster and data acquisition software is about $3.5M. The cost of a smaller scanner would have to be agreed upon with the chosen vendor and will depend on the number of units needed. An estimate of $1-1.5M is reasonable.

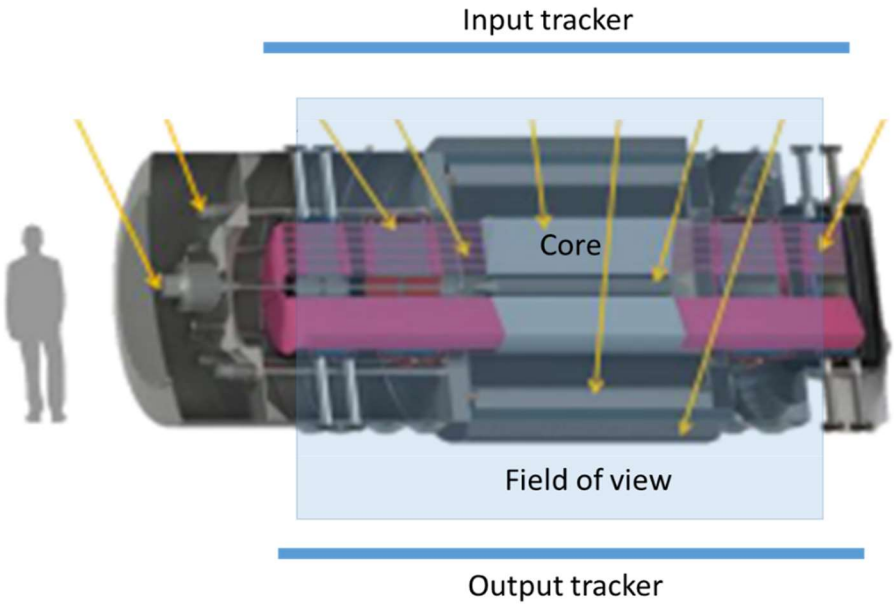

Figure 5-6. Schematic showing the field of view of a 16x16 foot^2 tracker overlying a conceptual drawing of Westinghouse's eVinci micro reactor.

5.2.2. X-ray transmission

The X-ray techniques use the generation of 4 MeV or 15 MeV X-rays as an interrogation source. The X-rays travel through the reactor and can interact in the fuel, structural, and shielding material. Some X-rays are absorbed and do not penetrate, some scatter and make it through with less energy,

and some do not scatter and pass through with their full energy. On the other side a radiation detector measures the X-rays and possibly their energy.

Measurement results are analyzed by assessing the number of X-rays that get through the system. The simplest technique is to measure the transmission fraction of the radiation which is the percent of full energy radiation that makes it through. If all the fuel is present, this fraction will remain the same at various points in the fuel cycle. If the fuel is absent, more radiation will pass through and the transmission fraction will change. If the fraction is the same at all positions around the microreactor the fuel is confirmed to be present.

Some complexity can be added to this technique to improve its capability. The size of the detector on the other side dictates how wide a field of view the measurement has and thus how large an area of fuel is measured at any one time. Multiple measurements may be required to measure all of the fuel, or sampling a fraction of the fuel may be satisfactory. The detector could be narrow to assay smaller amounts of fuel at a time, increasing the resolution at the expense of requiring more measurements and increased measurement time. Multiple narrow detectors could be placed next to each other so multiple measurements could be taken at the same time. This improved resolution will help locate where specifically the fuel is missing and increase the sensitivity. For example, if the measurement is sensitive to 10% missing fuel and is measuring the entire reactor of 1000kg of fuel, then up to 100kg can be removed before the diversion is identified. If a narrow section of 100kg is measured then only 10kg can be removed. Similarly, the shielding of the reactor has a similar effect on the radiation as the fuel. If the radiation detector or generator can be moved underneath the shielding, the sensitivity might for example go to 1% because the only thing affecting the transmission would be the fuel, not the fuel and the shielding. This approach would need to be incorporated into the reactor design as discussed in Chapter 4.

Another improvement would be energy spectroscopy. Many detector options detect the energy of the X-rays. Spent fuel will create gamma rays up to about 1.5 MeV that add background to the measurement. Having an energy threshold to ignore this signal and only measure the high energy X-rays from the generator will be important as the fuel burnup increases. As the X-rays scatter, they lose energy. A higher threshold will allow measurement of X-rays that have undergone minimal scatter or none at all.

5.2.3. X-ray radiography

X-ray radiography could be used to confirm the state of the fuel rod matrix inside the modular microreactor assembly. The design basis reactor specifications present formidable challenges to achieving this goal, mainly due to the 4-inch thick lead shield surrounding the reactor for gamma-ray shielding combined with the large areal density of the fuel rods themselves. The primary advantages of X-ray radiography are

1) High penetration capability of high-energy X-rays.
2) Ability to choose and adjust X-ray energy for penetration power and density contrast.
3) Commercial availability and support of generator and detector instrumentation.

The disadvantages are

1) High cost for detectors, generators, and associated support equipment, on the order of multiple-millions of dollars.
2) Large, bulky generators for high-energy applications, meaning in-situ radiography is difficult or impossible in tight areas.
3) High levels of shielding required for the needed energy and dose to penetrate the microreactor.

To choose an appropriate X-ray generator, we consulted with Varex Imaging, a manufacturer of commercial high-power generators for industrial-scale applications. High energy X-rays, greater than 1 MeV, are necessary to penetrate the assembly. Varex's highest-energy mobile-capable generator, the K15, was chosen. This generator has a maximum acceleration voltage of 15 MeV delivering a dose of 120 Gy/min at 1 m from the exit aperture. Typical applications for this class of generator are radiography of shipping containers packed with high-density materials and inspection of large solid-propellant rocket boosters for ballistic missiles and space vehicles. In these applications, a 1D collimated strip detector with 1 mm-sized pixels is used to scan through the object lengthwise to generate the radiograph within minutes. However, this microreactor application is at least 1-2 orders of magnitude higher in areal density than these typical applications, making direct comparison difficult. The K15 does have center-of-mass pivot point mounts, shown in Figure 5-7, allowing arbitrary orientation when mounted from e.g. an appropriate crane arm.

Figure 5-7. Varex Imaging K15 X-ray generator.

There are two primary areas of performance to evaluate: photon flux or brightness and spatial resolution. To calculate the expected X-ray flux through the reactor onto the detector, we first approximate the spectral flux per 1 MeV bin using a Bremsstrahlung spectrum scaled to the appropriate total flux to deliver the specified dose at 15 MeV operating energy. We estimate the attenuation for each 1 MeV-wide bin through various paths through the reactor using mass attenuation coefficients from the NIST X-COM database. In the horizontal direction, the two primary paths are through the central diameter of UO_2 fuel rod matrix, and directly adjacent to the fuel rod matrix, through the full shielding without fuel. We also consider measurement through the vertical axis of the reactor to establish the presence or absence of individual fuel rods.

In the horizontal view, we estimate that only approximately 10 photons/min/cm^2 would penetrate the full fuel rod assembly, which, combined with the expected background, is essentially opaque. However, we calculate that about 10^7 photons/min/cm^2 will penetrate the lead shielding and other non-fuel components of the reactor, in either the horizontal or vertical orientation. From these calculations we conclude that horizontal radial imaging would, at best, be able to discern the general hexagonal shape of the core by imaging through multiple angles, accounting for the partial attenuation through the shorter paths at the hexagon points. We also conclude that vertical axial

imaging, if achievable with space constraints and assuming there are not large amounts of unaccounted high-density material above or below the core, would be able to image and confirm the presence of individual fuel rods installed in the core. We estimate that the time required to characterize the core by a 2D image for the vertical view, collected by single element raster scanning, or a multi-angle slice through one plane of the core in the horizontal view, would require about 2-4 hours.

Spatial resolution is determined by four factors: the spot size of the generator, the effective magnification of the source-object-detector geometry if using linear or 2D imaging, the spatial resolution of the detector due to the element and collimator size, and scattering from other objects in the field of view. The K15 spot size is about 0.5-1 mm and sets a lower limit on the smallest resolvable feature size. Scattering is a concern primarily if the detector is an uncollimated 2D imager, e.g. a scintillator-coupled charge coupled device (CCD). If a single point detector or 1D line detector with heavy collimation is used instead, the effect of scattered photons is minimized. The detector element size has wide latitude, from sub-mm to greater than 1 cm, and may be chosen to suit the available flux at the detector plane. Given the estimated photon flux, we estimate that a 2 mm detector element is appropriate for this application, yielding an effective spatial resolution of about 2 mm.

Finally, we consider the practical costs of this technique. The K15 cost is approximately $2.5 million, and a custom-engineered detector system will cost between $200 k and $1 million, depending on the complexity. The system may designed as a mobile unit, integrated onto a trailer with integrated detector positioning crane, at a cost of approximately $1 million. Alternatively, it could be constructed as a permanent installation in a building at a variable cost, estimated between $500k and $1 million. Shielding is another critical consideration, especially if the unit is intended to be deployed to the field or installation site, and could add another several $100k or more. The final estimate for a fully mobile system is of order $5 million, which is likely far too expensive for multiple units, but may be acceptable at for example a single decommissioning facility or with one mobile unit for the entire US fleet of microreactors.

In summary, it is likely that X-ray radiography could provide verification of the presence of fuel rods in the microreactor core in a measurement time of hours, provided it can be measured through the vertical axis either with the reactor on its side before installation or after removal, or with the generator moved above the vertical reactor. Given the physical size of the generator, once the reactor is installed it may be more difficult to achieve some measurement configurations. Imaging through the side radial axis should give general confirmation of the hexagonal core shape but would be unable to verify the absence of individual fuel rods.

5.2.4. X-ray computed tomography

Computed tomography is the complex analysis of X-ray transmission as a function of position to create a 3D image of the core. It would use the same radiation generator and detector as the X-ray transmission measurement, but use medical imaging algorithms to combine the information into a reconstruction of the position of attenuating materials.

While computed tomography is a mature technique in other applications, we are not aware of a successful application to a scenario with significant shielding like a microreactor. It is likely that the shielding greatly complicates the measurement making it unfeasible.

5.2.5. Neutron transmission

Similar to X-ray transmission, neutron detectors can be placed on the opposite side of the reactor from a neutron generator. A Deuterium-Tritium neutron generator generates 14 MeV neutrons with an emission rate as high as 10^13 neutrons per second. The fraction of neutrons detected depends on the scattering interactions in the fuel and structural material. Removing the fuel will change these interactions and the transmission fraction. Again, the detector configuration can be adjusted to change the resolution of the measurement and the measurement time.

Fast neutron detection for spent nuclear fuel in dry casks is being studied using ^{4}He detectors [24]. These detectors work on scattering of fast neutrons with helium gas. As fast neutrons move through the gas, they undergo elastic scattering and transfer a fraction of their kinetic energy to the ^{4}He nucleus dependent on the scattering angle. After a series of events scintillation light is emitted which can be detected. Fast neutron detection can also be performed with plastic or liquid organic scintillators. All of these detection techniques potentially allow for energy spectroscopy of the detected neutrons which could be used to distinguish between the high energy DT generator neutrons and the lower energy fission product neutrons which need to be subtracted as background for this technique's application in the microreactor life cycle after operation. The alternative is thermal neutron detection, where the fast neutrons are moderated to low energy where they are very likely to undergo capture reactions in the detector.

This method is quite similar to the x-ray radiography method described in section 5.2.3. The neutron generator would be industrial scale and produce a high radiation field. The generator, facility, and shielding required would likely cost millions of dollars. The performance would also be similar, meaning that due to the large amount of shielding, precise results would be extremely difficult.

A recent study applied neutron backscatter measurements to the similar application of spent fuel casks [25]. Using a neutron generator with 10^{10} n/s emission rate, a missing bundle could be detected in a 2 hour measurement. The radiation is emitted and measured on the same side of the cask instead of transmitted through. In the study the fuel was not replaced by lead or steel which would make the method less effective. However, when combined with measures such as tamper indicating devices, the method may provide enough confidence despite this limitation.

5.2.6. Neutron radiography

Neutron radiography is the process of making an image with neutrons. Neutrons interact with the nucleus of the atom rather than the electrons. In contrast with X-rays, neutrons are attenuated by some light elements but penetrate many heavy elements. The attenuation of neutrons is dependent on the nuclear scattering and absorption cross-section of the material [26]. Some object features easily visible with neutron radiography and computed tomography may be very challenging or impossible to see with X-ray imaging techniques. Materials made of light elements often have low density and have negligible attenuation of X-rays. As a consequence, the images that neutrons produce after passing through an object will be particularly revealing of substances containing light elements which would be invisible with X-rays.

The core of a microreactor containing high Z uranium fuel is very dense. Hence high resolution neutron imaging of the core would not be feasible as neutrons would penetrate this material. The support structures and shielding material made of lower Z material could be imaged using neutrons.

5.2.7. Neutron computed tomography

Neutron computed tomography is a technique to derive maps of the neutron attenuation coefficient values of an object [27]. This technique has the ability to produce 3D images of the inner macroscopic structure and material composition of the item being studied. It is particularly useful when many layers of heavy metal need to be transmitted and lighter elements need to be detected. Because we are interested in measuring the heavy elements of nuclear fuel, this technique may not be ideal for our application.

5.2.8. Neutron active interrogation

Neutron active interrogation is often performed to measure uranium in other applications. The neutron generator could induce fission in the fresh uranium fuel and the induced fissions could be measured. The external neutron radiation would only need to penetrate into the fuel, not through the shielding a second time, so it may work better than the other techniques. The secondary radiation has an average energy of about 2 MeV and would have to penetrate the shielding. One benefit is that only neutrons emitted in the fuel close to the side of the reactor are likely to escape out that side, so measurements of the neutrons from this technique will measure a small section of fuel at once. The result is higher resolution measurements and higher sensitivity. However, the neutron generator itself will add significant background which must be accounted for and may make the technique unfeasible.

Another concern is the type of reactor. For the previously discussed techniques, differences in the microreactor type would not affect the measurement. For this technique, fast or thermal neutron spectrum reactors would have different measurement physics and results. Neutron induced fission is more likely at lower neutron energies. A thermal reactor has significant neutron moderator which would lower the interrogation neutrons' energy and greatly increase the probability of induced fission. The moderator may cause the technique to perform better because of more neutron generation, or may cause it to perform worse because the neutron penetrability across the core is lowered. Fully understanding issue will require further study.

5.3. Passive Measurement Techniques

5.3.1. Passive spent fuel radiation emission measurements

The gamma or neutron emissions from spent fuel can be measured to identify diversion of the fuel. The measurement can be taken at some beginning time, say, after reactor shutdown but before transportation to the disposal site, and then subsequent measurements can be compared to the first benchmark measurement. The measurement would likely be taken at many places along the outside of the reactor. If the fuel is removed, the measurement nearest the removed section would not match the expected value. The measurements would need to account for radioactive decay, either by computer modeling, repeated measurements at shorter time intervals to understand the rate of decay, or normalizing localized measurements to a general measurement of the entire reactor. For example, one measurement would be taken near each of the six fuel sections and divided by the sum of the six measurements to make six ratios. At a later date after radioactive decay, the individual measurements and the sum of measurements would decrease by the same fraction so the ratios would be the same if all the fuel was present. If some fuel was missing some or all ratios would not match. The method would likely still use computer modeling to estimate an expected count rate which would be used to identify if all of the fuel was missing, but this method would be much more

sensitive to small amounts of missing fuel which computer modeling may not detect due to its larger uncertainty. This method is sometimes called 'fingerprinting' and was explored for dry cask storage as described in Appendix C.

The major benefit of this method is that it is simple and it is very likely to work with minimal development. The equipment, external radiation detectors, are also relatively inexpensive, depending on the required performance. The radiation is emitted uniformly in the fuel. It is unlikely to travel across the core, so most of the radiation measured at one side is from the fuel on that side. This effect causes the measurement to be localized to smaller amounts of fuel. However, the sensitivity to fuel at the center of the reactor is likely low, most of the measured radiation will be from the outer layer of fuel closest to the radiation detectors.

5.3.2. Mass measurement

Load cells exist which could weigh the microreactor. A mass measurement is likely the simplest method, but is also easier to defeat. Should the fuel be removed, any material could be added at any location to balance the loss. Overall, it does add significant difficulty in removing fuel undetected and may be the most feasible technique. Industrial scales can easily measure up to 100,000 lbs or more [28]. The uncertainty of the measurement will need to be understood, as the fuel may be a small percent of the total weight due to the large amount of shielding. It would be ideal if the scale could be integrated into the reactor to weigh the fuel only.

5.3.3. Fresh fuel passive neutron emission

Fresh uranium fuel does emit some small amount of neutrons through spontaneous fission. Measurement systems for single fresh fuel assemblies taking advantage of this phenomenon are being explored in active research. It is possible that this small amount of emission may still be detectable, especially with a large enough radiation detector or large enough mass of fuel. Because the neutron emission rate is low it will be especially important for this technique to be integrated underneath the shielding.

This technique has several benefits. Because the radiation source is the fuel itself, expensive radiation generators are not necessary. The detection equipment could be smaller and less expensive because it is so closely coupled to the fuel and does not need to account for transmission through the shielding. Most reactors have in-core neutron instrumentation, so those systems could be used or modified for this purpose with minimal reactor changes. However this does require integration with the reactor's design before a reactor is built. Due to these benefits and a lack of published literature demonstrating similar techniques, the feasibility of this technique was calculated in detail in Chapter 6. The evaluation assumed 6 fuel channels of the 2,112 in the MegaPower reactor design were replaced with boron lined detectors. After accounting for background due to cosmic rays, a 224 minute measurement could detect 5.6% or more of the fuel being removed in the conservative scenario that the diverter targeted the fuel furthest from the detectors. This corresponds to 250.1kg of uranium or 49kg of U-235 in Low Enriched Uranium. The cost of this technique would be on the order of $50,000 which is much lower than the millions of dollars for other techniques.

5.3.4. Gamma and neutron imaging

Gamma and neutron imaging have been developed for nuclear radiation measurement applications. They have been applied to dry cask measurements. They use a pixelated radiation detector which can

detect the energy and location of the same radiation particle twice. By combining the starting and ending position and energy, they can recreate the initial direction of the particle before it hit the detector. Overlaying this information on an image can show the direction radiation is coming from and help to detect the location of radioactive material. Another method is a coded aperture mask which is used to identify the initial direction of radiation. However the resolution of these methods is usually poor, and the large amount of microreactor shielding will make it even poorer. Knowing the direction of the radiation provides little benefit for our application compared to gross radiation counting, but adds significant cost and complexity.

5.3.5. Passive emission tomography

Passive emission tomography is a very impressive technique which has been developed for spent fuel assemblies without shielding. It independently identifies the location of nuclear material with high resolution by measuring the gamma emission with many collimated detectors. The technique is quite complex and has required significant development to reach its current state. Unfortunately, the large amount of shielding for a microreactor likely makes it very difficult to achieve useful results, especially without significant further development.

5.4. Application to the Life Cycle Framework

There are many considerations for the various technical options in their application to MC&A at each stage of the microreactor life cycle. The potential applications, costs, measurement times, and performance are listed to allow comparison and a general understanding of potential solutions to the problem. This information should be discussed with the NRC and microreactor vendors to better understand the feasibility of certain solutions, identify concerns and preferences, and determine which solutions, if any, should be developed further.

First, the safeguards by design options are summarized. The shielding around the microreactor adds significant difficulty in confirming the presence of the fuel. The shielding's purpose is to reduce the dose rate due to spent fuel, but before operation the fuel is fresh and the radiological hazard is negligible. If the shielding can be removed it may be much easier to confirm the presence of the fuel, potentially avoiding the need for radiation measurements at all. The next safeguards by design option is to use any in-core neutron instrumentation as a measurement of the fuel to confirm its presence. This may not add any cost or complexity to perform MC&A which are attractive characteristics. Finally, radiation measurement technology could be incorporated underneath the shielding. This would improve performance and reduce the size and cost of the measurement equipment. It is possible that only about 2 inches of space would be needed, but it does add significant complexity and the cost and risk of this option would need to be discussed with the microreactor vendors. Weighing the reactor and the spent fuel inside is another similar option which has minimal cost.

Table 5-3 below summarizes the various techniques and their issues. Note the values are rough estimates to use as an initial discussion point and general understanding. The uncertainty of these estimates is high, and in some cases insufficient information is available to make an estimate. The cost, time, and performance are normally tradeoffs, for example an increase in measurement time can improve performance. Typically new NDA techniques and applications undergo years or decades of research and development which improve their practicality, performance, and cost.

Table 5-3. Summary of radiography and radiation measurement techniques.

Technique	Microreactor life cycle phase applicability	Cost ($10k, $100k, $1m, $10m)	Measurement time (hours, days, weeks)	Performance (sensitivity to missing fuel, or image resolution)
External radiation interrogation				
External radiography - muon	All	$1m for the muon tracker	1 week	Medium resolution imaging
External radiography – X-ray	All	$2m for the x-ray generator, $100k-$1m for facility and shielding needs, and $100k for the detector	hours-days	Low resolution imaging
External radiography – Neutron	All	$1m for the neutron generator and facility, $100k-$1m for the detector	hours-days	Low resolution imaging, or medium sensitivity to missing fuel
External radiography, internal radiation detector - Neutron	All	$1/10^{th}$ that of external neutron radiography.	Hours-days	Low resolution imaging, or medium sensitivity to missing fuel
Passive measurement of fresh fuel				
In-core neutron instrumentation	Before operation	$50k for independent equipment, Potentially $0 using operator's equipment	224 minutes	Detection of 5.6% or more fuel removed
Passive measurement of spent fuel				
In-core neutron instrumentation	After operation	$50k for independent equipment. Potentially $0 using operator's equipment	Hours-days	High sensitivity to missing fuel
Non-radiation based techniques				

Removing shielding to verify fuel	Before operation	$0 in equipment	Hours-days	High sensitivity, direct visual inspection
Weight measurement	All	$10k-$100k	seconds	High sensitivity, but easily spoofed

6. FEASIBILITY OF IN-CORE NEUTRON ASSAY

In-core neutron instrumentation was evaluated in further detail for its feasibility. In core instrumentation has a significant advantage by being underneath the core shielding, greatly increasing the efficiency of detectors. It could either utilize instrumentation already integrated for reactor operation, or application-specific instrumentation could be added with minimal impact to the reactor. The method would use mature neutron detector technology which is highly reliable. The neutron source term is the passive emissions from spontaneous fission and (α,n) reactions in the uranium fuel. Such simple technology utilizing the fuel's own radiation signature results in a simple measurement approach with minimal cost, on the order of $50,000. This analysis focused on fresh fuel but spent fuel will be evaluated in the future. Spent fuel is typically measured with fission chambers which can withstand the high gamma doses. The lower efficiency of the fission chamber is balanced by the higher neutron emission rate of spent fuel, so the overall measurement approach would be quite similar to the approach demonstrated here.

The physics basis for fresh fuel (before reactor startup) is that the 4,500kg of U in the core emits 67,906 neutrons per second from spontaneous fission of U-238 and (α,n) reactions on oxygen. Measurement of these neutrons is a direct signature of the presence of the uranium.

Three neutronics metrics were evaluated to determine feasibility of the measurement technique:

1. The detection efficiency must be reasonably uniform across the core.
2. The count rate must be large enough such that the number of counts recorded in an acceptable measurement time is reasonable. The space in the reactor core dedicated to the instrumentation must be limited to minimize impact on the core design.
3. The uncertainty of the background count rate should be small enough that any uncertainty introduced by background subtraction is negligible.

6.1. Benchmarking – UNCL

This analysis was performed primarily using MCNP radiation transport simulations. Simulations of passive neutron measurements of a BWR-type fuel assembly were used to benchmark the simulation performance and demonstrate the accuracy of the simulations. The measurement was performed with a uranium neutron coincidence collar (UNCL)[29,30]. The 6x6 BWR fuel assembly consists of 2.3% enriched uranium oxide. The UNCL uses an americium-lithium (α,n) source to produce interrogation neutrons to induce fission in the U-235. The neutrons then thermalize in the polyethylene and are detected by He-3 based neutron detectors. This measurement is representative of the microreactor scenario because it captures two key aspects: uranium neutron interactions and thermal neutron detection. The measurement and simulation are shown in Figure 6-1.

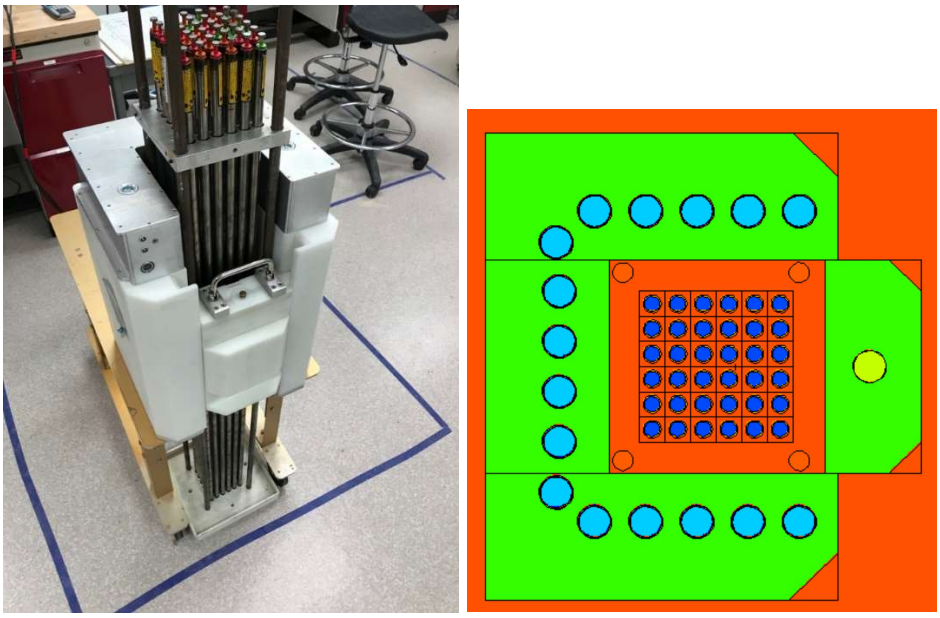

Figure 6-1. UNCL and BWR fuel experimental configuration (left). Top down view of MCNP model of UNCL and BWR fuel (right).

The simulated neutron count rate agreed with the measured count rate to within 6%. This demonstrates that the application of MCNP to uranium and neutron measurements is sufficiently accurate for this feasibility study.

6.2. Detector Design and Placement

There are any number of possible detector configurations which could be evaluated. The layout chosen for this work was to place the detectors in the reactor fuel channels, each replacing an individual fuel rod. Placement in the channels is consistent with a reactor's in-core instrumentation so these channels are likely to already exist as part of a core design. Placing the detectors within the fuel maximizes geometric detection efficiency and provides the most uniform efficiency profile. Six detectors, one per fuel 'wedge' were chosen to follow the reactor's hexagonal symmetry. The impact on the fuel is minimal since only 6 out of 2,112 fuel channels are replaced. Six detectors also minimizes equipment cost while allowing the measurement to have spatial resolution and redundancies for equipment failure.

The detectors were chosen to be boron lined proportional counters. Boron detectors are commercially available for use in nuclear reactors [31]. The detectors can be fabricated in various sizes. A simple single-layer of 2 um thickness of boron was assumed. Note that more complex, higher efficiency boron lined detectors are available. Each detector fits in a single channel, so they have an outer diameter of 1.575 cm and are the length of the core, 150 cm.

The detectors' distance from the center of the reactor was optimized to flatten the detection efficiency profile as a function of uranium location. The objective is to ensure that all fuel contributes equally to the count rate to maximize detection sensitivity of uranium mass. This optimization was performed in the radial dimension only due to the reactor's symmetry. The potential detector locations are the fuel channels along the center line, labeled as position index 1 to 24 for the top left 'wedge' and -1 to -24 for the bottom right 'wedge', Figure 6-2.

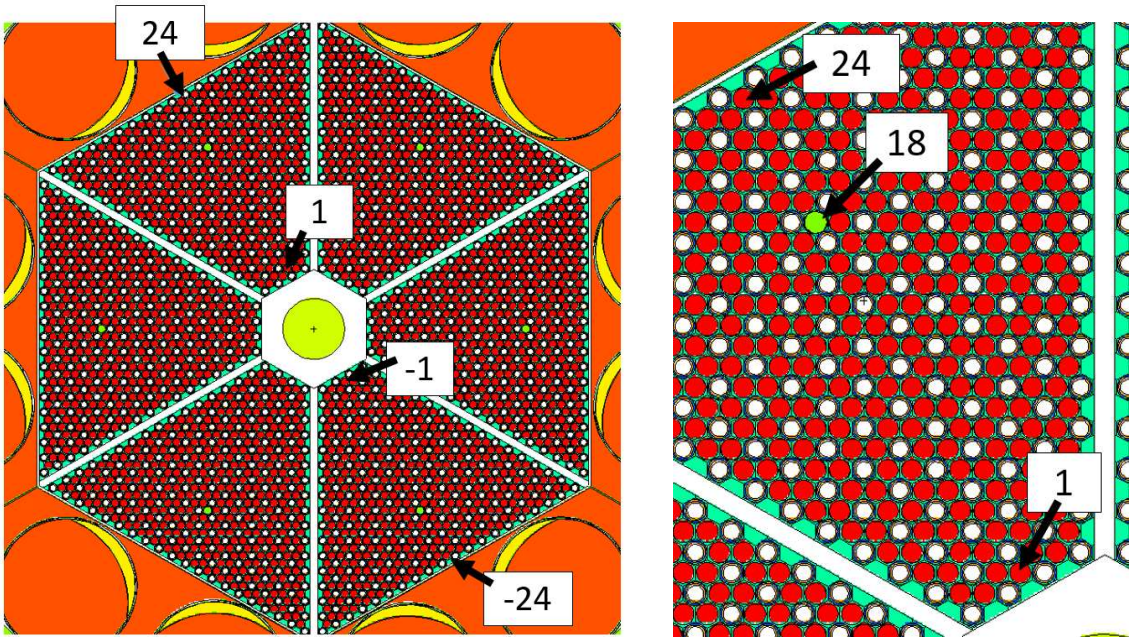

Figure 6-2. Fuel channel index from 1-24 on the top left 'wedge' and -1 to -24 on the bottom right 'wedge' [left]. Position of the location-optimized detector at position 18 [right].

The detection efficiency as a function of fuel pin location was found. This was repeated for the detector located at each fuel channel. The efficiency of the close detector and the far detector were averaged (the other detectors were omitted due to symmetry). Then, the ratio of the fuel pin with the highest efficiency to the lowest efficiency was found. This indicates the flatness of the efficiency profile. The detector position with the smallest difference between high and low efficiency was found to be position 18. This was chosen as the detector design for the rest of the analysis. The ratio of high to low efficiencies for all detector positions is shown in Table 6-1. The efficiency profile when the detector is at position 18 is shown in Figure 6-3.

Table 6-1. Maximum over minimum efficiency per fuel channel as a function of detector position

Detector position	Max./min. efficiency
24	2.23
22	2.16
21	2.30
19	1.92
18	**1.81**
16	1.99
15	2.18
13	2.02

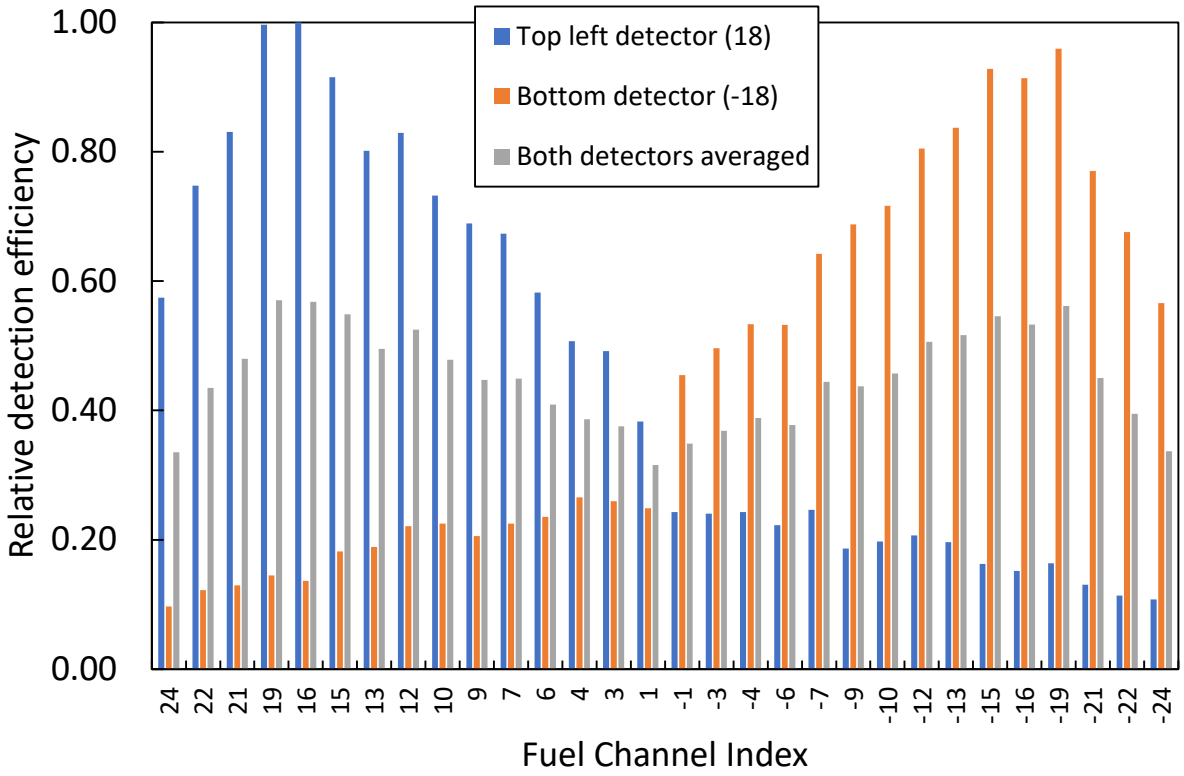

Figure 6-3. Relative detection efficiency per fuel channel when the detector is in its optimized position (channel number 18).

The UNCL is a widely used international safeguards instrument. The UNCL's maximum / minimum efficiency is, coincidentally, also approximately 1.8 (29). Therefore, the maximum / minimum efficiency of 1.8 is sufficiently low to determine that the detection efficiency is reasonably flat across the core. This result satisfies the first feasibility metric.

6.3. Count Rate From Fuel

MCNP was used to calculate the count rate from the nuclear fuel. The microreactor was simulated with the source term being spontaneous fission and (α,n) neutrons within the fuel rods. The detectors were also modeled and the detection efficiency was tallied. The total neutron count rate is summed over each detector of the detection efficiency multiplied by the neutron emission rate. The nuclear data and microreactor characteristics related to neutron production in the fuel are given in Table 6-2. The simulation results and total count rate are given in Table 6-3.

Table 6-2. Neutron emission per isotope in the Megapower core.

Isotope	Mass (kg)	Specific production (n/s-g) Spontaneous fission	(α,n)	Neutron emission (n/s) Spontaneous fission	(α,n)
U-234	6.78	5.02E-3	3.0	3.40E+1	2.03E+4
U-235	887	2.99E-4	7.10E-4	2.65E+2	6.30E+2
U-238	3,596	1.36E-2	8.30E-5	4.89E+4	2.98E+2
Total	4,489	-	-	49,205	21,252

Table 6-3. Detection efficiency and total count rate

Average detection efficiency (%)		
Spontaneous fission	(α,n)	Total count rate (n/s)
1.32E-4 ±2.7%	2.77E-4 ±2.7%	0.743 ±2.7%

The second metric is that the count rate must be large enough such that the number of counts recorded in an acceptable measurement time is reasonable. A count total of 10,000 counts is typically used because it corresponds to a 1-sigma relative statistical uncertainty of 1%, per the formula below. In the formula σ is the 1-sigma relative statistical uncertainty and *n* is the number of counts.

$$\sigma_{rel.} = \frac{\sqrt{n}}{n}$$

The count rate of 0.743 n/s will result in 10,000 counts in a measurement time of 3 hours and 44 minutes. This count time is reasonable in the various measurement scenarios where quantification of the fuel would be valuable. For example, if the reactor is shipped to a new location or its ownership changes the 4 hour measurement could be performed overnight or while other activities are occurring at the site.

The second aspect of the metric, that the space in the reactor core dedicated to the instrumentation must be limited to minimize impact on the core design, is also satisfied due to the small number of reactor channels required to produce a sufficiently high count rate.

6.4. Background Count Rate From Cosmic Rays

In real-world application of the technique the background rate must be subtracted to find the count rate from the nuclear material. The random variation in the background count rate introduces uncertainty in the background subtraction and ultimately the count rate of the nuclear material. The random variation in background count rate is the absolute background count rate multiplied by the relative fluctuation.

Cosmic ray flux varies with many factors, including the sun's activity cycle. The uncertainty from the cosmic ray background is larger than just the statistical uncertainty due to this fluctuation. In this work an uncertainty (random variation) of +-25.7% (3σ) is determined from the range of fluctuation in measurement data collected over a period of 36 years (4 solar cycles) [32]. The uncertainty could also be reduced by various techniques including accounting for the solar cycle or taking more frequent background measurements.

The background count rate from cosmic rays was simulated in MCNP. This simulation method was previously shown to agree with measurements within 39% [33]. This agreement, while somewhat worse than the UNCL benchmarking, is quite accurate given the complexity of cosmic ray neutron production. The agreement is sufficient to give an estimate of the magnitude of the background count rate. In real-world application the background count rate would be measured which would result in a more accurate value. Also, the cosmic ray count rate is small relative to the count rate from the fuel, so an error in the cosmic ray count rate of this magnitude would not affect a determination of feasibility. Thus the simulation is accepted as accurate for the calculations of this work.

The real-world background count rate consists of terrestrial and cosmic sources. The simulation does not include terrestrial sources because they are heavily attenuated by the reactor's shielding. In the benchmarking the simulations were 39% higher than the measurements so the simulation result is a conservatively high count rate. The cosmic rays produce secondary neutrons through high energy spallations of primary particles. These primary particles can be highly penetrating, and the high density shielding and fuel of the reactor may actually increase cosmic ray neutrons instead of decrease it. A significant question which is answered by this work is whether the reactor shielding is effective at reducing cosmic ray neutron flux, or if instead the high Z materials at the center of the reactor cause large spallations which produce a high neutron flux.

The cosmic ray simulation is explained in detail in other work [33]. The MCNP cosmic ray source at the top of the Earth's atmosphere was transported down through the atmosphere to the altitude of Los Alamos, NM (2200m). The intensity, direction, and energy of the 15 nuclear particles which make up the ground level cosmic ray source term was tallied. This simulation was performed in a 2kmx2km area, so a second simulation was performed to transport this source term to a microreactor sized box and incorporate a concrete ground. The detailed information of the particles was tallied again for this box and used to create a source term which can be used without repeating all the previous transport. Finally, the microreactor simulation was placed inside the box and this source term was used to calculate the count rate from the cosmic rays. The summary of these steps is shown in Figure 6-4.

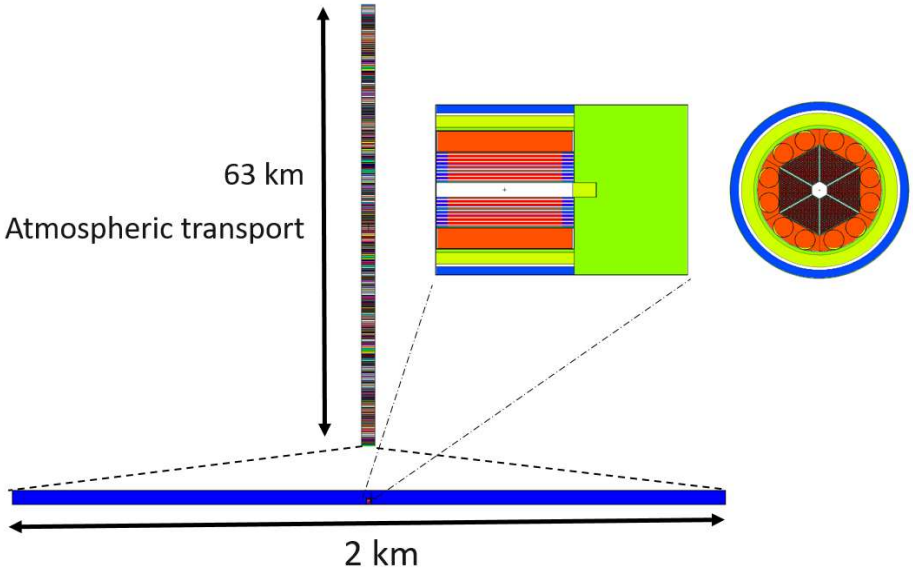

Figure 6-4. Visual of the cosmic ray transport. The steps were (1) through 63km of atmosphere, (2) to a box at the center of a 2km square, and (3) started with the microreactor inside the box.

The result was a count rate of 0.00245 neutron counts per second from cosmic rays. The uncertainty is (0.00245 * 0.257) = 0.000632 counts per second. The count rate from the uranium, 0.743 n/s, is 303 times greater than that of the cosmic rays, and 1,170 times greater than the uncertainty of the cosmic ray counts. Therefore the background count rate introduces a negligible uncertainty and the third metric for feasibility is satisfied.

6.5. Discussion

The results of this analysis have revealed several interesting physics concepts which will be useful in improving future designs.

The choice of using a single fuel channel per detector restricts the size of the detectors and lowers their efficiency significantly. Standard detectors without space limitations are often chosen to be much larger to increase their efficiency. Larger detectors would be advantageous if possible during integration into a specific reactor design. Similarly, having more detectors will improve the measurement performance by further flattening the efficiency profile across the reactor. A larger number of evenly spaced detectors would reduce the maximum distance between fuel and detector, reducing the effectiveness of targeted diversion by ensuring a more uniform measurement of all of the fuel. However, both of these preferences conflict with a design goal of minimizing impact on the reactor design, so a solution would need to balance both considerations.

The results of the detector placement optimization suggest that the detection efficiency is quite uniform across the reactor. The 6 detectors are a good initial design to ensure that the extreme maximum and minimum count rates do not differ greatly from the average count rate. The maximum and minimum were found to be only +-30% from the average. This is a useful feature because the detectors are nearly uniformly sensitive to all of the fuel. While a +-30% range might seem large, in similar NDA measurements the drop off is much larger and the interrogation less uniform. For example, some dry storage cask techniques can only measure the outer fuel bundles. An important physics aspect of this feature is that the reactor is fast. Fast neutrons are more highly penetrating than thermal neutrons, so they can more easily traverse the reactor to reach the detectors. A thermal neutron core design, for example a LWR or graphite moderated reactor, would have much less uniform interrogation and the technique would have a larger diversion sensitivity

6.6. Conclusions and Future Work

This investigation demonstrated that the use of in-core neutron detectors is a feasible approach to quantitatively assay the nuclear material mass of microreactors. In-core detectors have physics advantages which result in an accurate assay with minimal equipment costs. This approach is especially valuable if existing operator in-core equipment can be utilized. The equipment cost is estimated to be on the order of $50,000. With a minor impact to core design, a measurement time of 3 hours and 44 minutes is feasible. The method uniformly assays the fuel throughout the core and is minimally impacted by background. The results suggest that the method's general performance is typical for neutron based NDA techniques and could likely be improved further.

The approach was demonstrated for fresh fuel before reactor operation, but expansion to spent fuel post operation will be pursued in future work. This analysis made several simplifying assumptions to demonstrate feasibility, but future work will also include further optimization of detector design, detector placement, and the quantity of detectors. Finally, experimental demonstration of this technique at a real world demonstration microreactor such as MARVEL would be valuable to develop the technology in real-world conditions.

7. CONCLUSIONS

This work discusses the concerns of implementing US domestic Material Control and Accounting required by 10CFR74 in microreactors, which are an advanced reactor type being developed for deployment in the near term. Current regulations are designed for large traditional LWRs and are not easily applied to microreactors. The first license application has already been submitted. The licensing process will clarify the requirements for microreactors. Various MC&A concerns were discussed in Chapter 3. The primary focus of this report is nondestructive assay of the fuel for MC&A. The regulations allow item counting to satisfy physical inventories. Still, there may be other scenarios where measurements would be valuable. Reactor ownership may be transferred or continuity of knowledge may be lost during the multiple transportations and remote operation proposed by vendors. The cores are designed to be sealed and operated for decades. Finally, there is no current disposal path for a microreactor, so decades long temporary storage may be relied on similar to spent fuel casks. Any of these scenarios could benefit greatly from a method to measure the fuel.

The major technical challenges are that the fuel is sealed in the reactor core so regular access is difficult or impossible, and that the core has thick radiation shielding making external measurements difficult. A variety of techniques may confirm the presence of the nuclear material while the core remains sealed. The techniques were identified from medical imaging, spent fuel dry storage casks, international nuclear safeguards, and the nuclear industry. They range from simple and inexpensive, such as weighing, opening the shielding, or using the reactor's own radiation instrumentation, to medium cost radiation detectors, to expensive full external radiography systems. The techniques have different costs, capabilities and applicability, which were identified. Seals and surveillance may also be sufficient or used in combination with these techniques to provide this confirmation.

One highly promising technique was utilizing in-core neutron instrumentation either specially added or already planned for the reactor's operators. The feasibility of this technique was calculated in detail. The instrumentation would be low cost compared to the other options, on the order of $50,000 if added specifically for this use. A measurement would take 3 hours and 44 minutes and be able uniformly assay the reactor core.

Overall, this work discusses the MC&A regulatory requirements and their application to microreactors. The feasibility of technical approaches to measuring a microreactor's fuel was evaluated. The results of this work can be further developed into solutions and approaches for microreactor MC&A, contributing to the successful deployment of microreactors in the near term.

APPENDIX A. CURRENT NRC APPROACH TO MICROREACTOR REGULATION

The ARS program is tasked with supporting the deployment of advanced reactors in the near term. The development of 10CFR53, Risk-Informed, Technology Inclusive Regulatory Framework for Advanced Reactors, is beyond the immediate scope of this work. However, this may be the regulation under which the majority of microreactors are licensed, and so this work may have significant value in satisfying those regulations as well. In addition, the NRC was directed by the Commission to inform their rulemaking with lessons learned from early advanced reactor reviews, such as the ones ARS is tasked with supporting [SECY-20-0032]. Thus this work may influence the regulations developed in 10CFR53. The NRC approach to regulating microreactors and the current status of 10CFR53 development is described in this appendix.

Currently reactors can be licensed under 10CFR50 and 10CFR52. These were designed for large light water reactors and are not easily adaptable to advanced reactor concepts including microreactors. Advanced reactors are licensed by these paths with the use of many exceptions. The NRC considers exceptions an undesirable method and their use is part of the motivation for developing 10CFR53 as the preferred path for advanced reactor licensing [SECY-20-0032].

The major driver of development of 10CFR53 is the Nuclear Energy Infrastructure Modernization Act (NEIMA), signed into law in 2019. The act requires the NRC to develop a framework to regulate advanced nuclear reactors by the end of 2027. NEIMA specifies that the regulations should be technology-inclusive, which it defines as 'flexible and practicable to a variety of reactor technologies' and using 'risk-informed and performance-based techniques'. While regulations at the 10CFR level are typically broad, the proposed 10CFR53 text is clearly more applicable than the current regulations to the microreactor MC&A issues of being transported and having a sealed core. This work will support the NRC by highlighting and addressing this issue.

In SECY-20-0032, April 12, 2020, the NRC staff requests the NRC Commission's approval of their plan for advanced reactor rulemaking. In the Commission's response on October 2, 2020, the plan was approved with two important points. First, publication of the rule should occur by October 2024, moving up the timeline by 3 years. Second, the staff should inform its rulemaking with lessons learned from early advanced reactor reviews. In supporting the near term deployment of microreactors, this work will likely also support the development of 10CFR53. The vendor Oklo has submitted a microreactor Combined Construction and Operating License (COL) under 10CFR52. Westinghouse has notified the NRC of their intent to engage in regulatory interactions with their eVinci design and have responded to the NRC Regulatory Issue Summary, although Oklo's submission of a COL is much further into the process.

The NRC has released preliminary rule language for 10CFR53 for public comment. One relevant section is 53.20, Safety Objectives. The first sentence is 'Each advanced nuclear plant must be designed, constructed, operated, and decommissioned such that there is reasonable assurance of adequate protection of the public health and safety and the common defense and security'. The direct specification of a safety and security requirement related to decommissioning contrasts with 10CFR50 and 10CFR52 which are primarily focused on the licensee's ability and requirement to decommission. Decommissioning is specified in 10CFR52 to take no more than 60 years. While 10CFR53 may have different requirements, 60 years illustrates the significant time period over which the nuclear material must be kept safe and secure. Ensuring the presence of the nuclear material for

MC&A over this time period may be accomplished by radiography. Radiography typically functions the same at year 1 as at year 60 because radiography is more direct and less complex than the use of computer codes to extrapolate out the nuclear material content based on simulations.

The second proposed sentence of 53.20 states that 'each advanced nuclear plant must take such additional measures to protect public health and minimize danger to life or property as may be reasonable when considering technology changes, economic costs, operating experience, or other factors identified in the assessments performed under the facility safety program required by 53.80'. Radiography is a nondestructive assay technique which is completely external to the reactor. In other applications radiography can have a very low recurring cost. By verifying the presence of the fuel over long periods of time, radiography may satisfy this requirement.

APPENDIX B. INDUSTRIAL AND MEDICAL RADIOGRAPHY TECHNIQUES

This section is a review of radiography as applied in medicine and industry. Radiography is the oldest and most common diagnostic imaging technique [B1,B2]. During medical radiography, typically X-rays are directed to the area of interest allowing it to pass through the target organ and then captured behind the flat X-ray film to produce a 2D image [B3]. Industrial radiography determines features inside of objects that are otherwise difficult to access. This appendix reviews various radiography techniques.

B.1. Tomography

Tomography or computed tomography (CT) is an imaging system that produces cross-sectional images or "slices" of anatomy. These images are used for a variety of diagnostic and therapeutic purposes in the medical industry. In this technique, as X-rays pass through the body, they are absorbed or reflected at different levels. A patient lies on a motorized platform while a computerized axial tomography (CAT) scanner rotates 360 degrees around the patient, taking X-ray images. A computer combines these images into a two-dimensional view of the scanned area, or slice [B4]. This technique is advantageous because it is useful for soft tissue scanning and can allow for precision down to a millimeter. A disadvantage of this technique is the large dose of radiation to the patient.

In tomography and computed tomography, 2D projections of 3D images are formed. In tomography, an X-ray source and linear detector array (LDA) scan vertically past a stationary object. However, in CT, a rotating object sits between a stationary X-ray source and LDA as shown in Figure B-1.

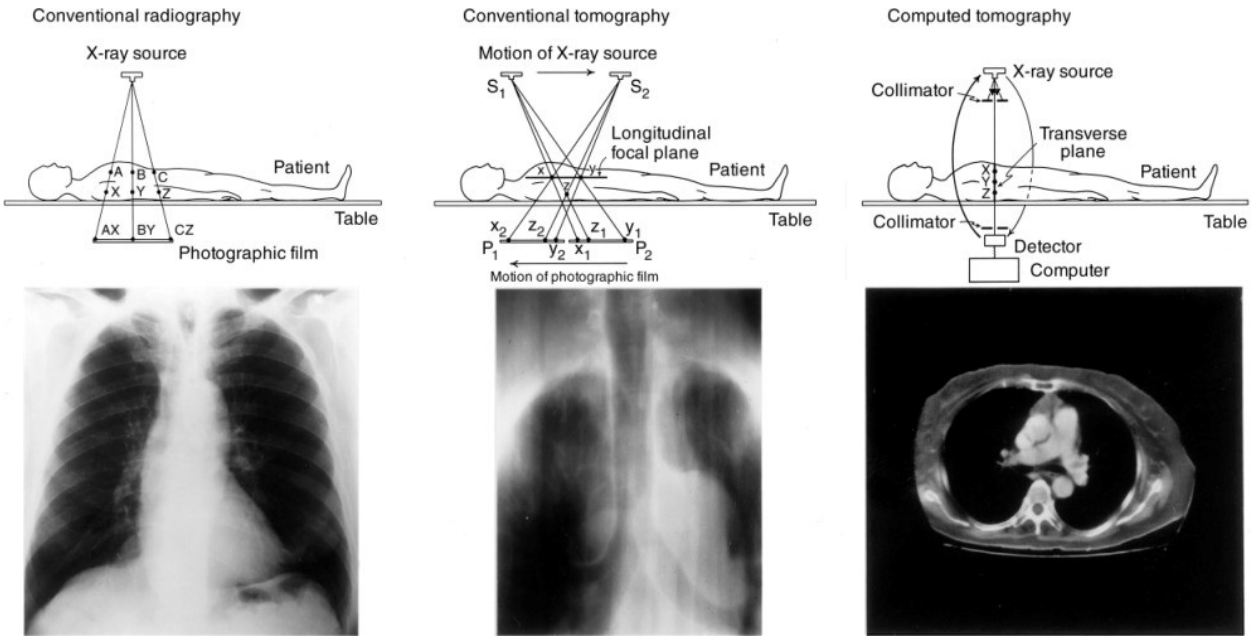

Figure B-1. Difference in types of medical radiography [B5].

B.2. Magnetic Resonance Imaging (MRI)

Magnetic Resonance Imaging (MRI) is a 3D imaging procedure that uses a strong magnetic field, 1.5 to 3 Tesla, to magnetize protons in the tissues of the body. The hydrogen nucleus is a single positively charged proton which generates a small magnetic field or moment when it spins. This phenomenon is nuclear magnetic resonance (NMR) which is the physics basis of an MRI [B2]. RF excitation of the protons results in energy absorption and subsequent re-emission of RF signals, which are detected and processed to reveal the magnetic characteristics of tissues displayed as a grayscale image. Pulse sequences specifically generate tissue contrast differences; typically, several sequences are acquired for a specific MRI study [B1]. The magnetic field across the body-sized sample is intentionally made non-uniform by superimposing additional magnetic field gradients that can be switched on and off rapidly [B6]. NMR equipment consists of a strong magnet, a radio transmitter and receiver. The advantages of MRI's are they are non-invasive, radiation – free, and provide precise imaging of target areas. MRI disadvantages are their high cost and long measurement time[B7].

B.3. Molecular Imaging

Molecular imaging uses tracers tagged with radioactive materials that are injected into the patient and are redistributed according to metabolic activity. A scintillation camera measures where the radiation is emitted from to create an image localizing the tracer. The measurement is acquired over a period of time, typically minutes to hours, and image sequences can be generated as a function of time, for example in first-pass bolus tracking and gated cardiac imaging [B7].

An example of molecular imaging is Positron Emission Tomography (PET). PET imaging uses positron emitters to produce annihilation photons. The positron emitters are attached to a metabolic agent and redistributed in the body. Two oppositely directed gamma-ray photons are created and form a "line integral" of activity from which a tomographic slice can be determined [B7].

B.4. Proton Radiography

Charged particle radiography using 800 MeV protons has been developed at Los Alamos National Laboratory. The protons are used as a radiographic probe for the diagnosis of explosively-driven dynamic-events in support of the LANL stockpile stewardship program [B8]. Protons have proven far superior to high energy X-rays for flash radiography because of their long mean free path, good position resolution, and low scatter background [B9].

The LANSCE accelerator produces an 800 MeV H-proton beam of macro pulses with widths of up to 1 ms and a rate of 120 Hz which corresponds to a spacing of 8.33 ms [B9]. The protons are delivered though a beam line that consists of a set of phosphor screens viewed by CCD cameras for beam monitoring and alignment, a strip line detector for measuring the time structure of the beam, a fast transformer for measuring the beam pulse intensity, a set of upstream quadrupole magnets for adjusting the angle position correlation of the beam on the sample to control chromatic aberrations, and a mechanical assembly that can insert any one of a set of tantalum diffusers to control beam spot size on the target.

In proton radiography two components contribute to the attenuation. The first term is due to nuclear scattering and absorption and the second is due to Coulomb multiple scattering [B10]. Magnetic lenses are used to restore the position resolution lost due to the Coulomb multiple

scattering. The ratio of images in a two lens proton radiography system can separate the loss of flux due to multiple scattering from the nuclear attenuation loss. If the multiple scattering angular distribution is given by a Gaussian, the transmission through an aperture, θ_c, for an object of thickness, z, is given by:

$$t_c = e^{-\kappa/\lambda}\,(1 - e^{-\kappa/z}) \text{ where } \kappa = \frac{\theta_c^2 p^2 \beta^2 X_0}{(14.1\ MeV)^2}$$

$$\text{and } \lambda = \frac{1}{p\sigma_A}$$

θc is the angular acceptance of the lens, p is the proton momentum in units of MeV/c, β is the proton velocity in units of the velocity of light, and X_0 is the radiation length in the same units as z [B10].

Proton radiography can provide <50μm position resolution for objects of the scale of 5 cm and areal densities of 10 g/cm², such as uranium oxide or thorium oxide. The generated radiation field can be larger than 200 Gy/h at 30 cm from the fuel rod because of the short exposure times and long standoff where the cameras and scintillator are 12 m from the object location [B9].

Figure B-2 shows tomographs of fuel pellets obtained with proton radiography. In the figure, (a) shows the texture in the thick thoria pellets, (b) and (d) the sensitivity of protons to 60 μm features, and (c) the ability to quantitatively measure density. The determination of density of the pellets in (c) was within a few percent of the measured densities of the sintered samples [B9].

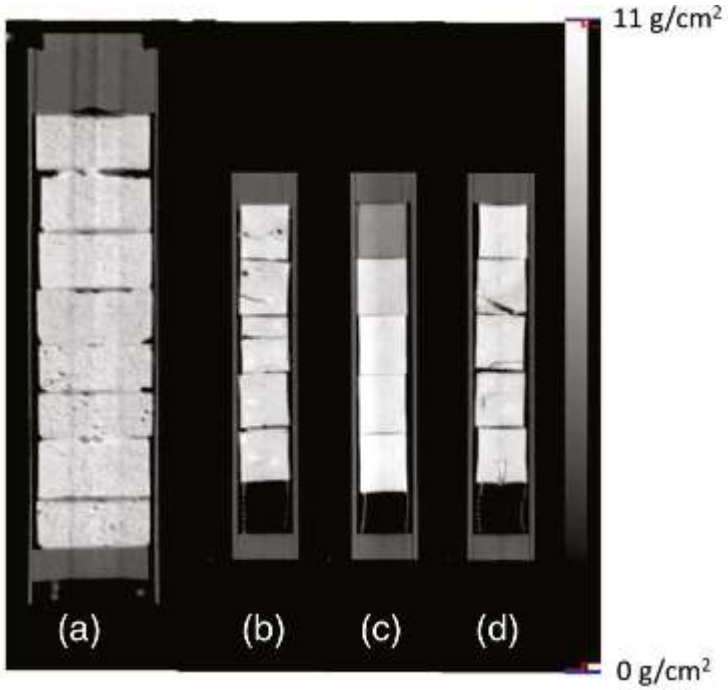

Figure B-2. Center slices from fuel pellet proton radiography tomographs. A density scale bar is shown on the right [B9].

Many new proton radiography capabilities are being studied. Dynamic experiments have shown that proton radiography can be used to study detonation propagation in high explosives, armor penetration, and instability growth in shocked and accelerated interfaces. In static experiments, radiography of

surrogate fuel rods, and casting experiments to study metal solidification dynamics, continuous radiography can create a movie of a self-propagating high temperature reaction [B9].

B.5. Electron Radiography

Los Alamos National Laboratory in collaboration with the Idaho Accelerator Center have developed an inexpensive and portable electron radiography system. This system has been designed to use 30 MeV electrons to radiograph thin static and dynamic objects [B8]. This system is expected to provide density measurements for static and dynamic objects with 0.01–1.0 g/cm^2 areal densities with an RMS spatial resolution of about 100 μm.

A Varian Clinac 2500 waveguide was recommissioned with a 5.5 MW CPI peak power klystron, producing a 20 μs S-band microwave pulse of 2.8 GHz. The accelerator is capable of delivering a pulsed electron beam with energies between 5 MeV and 32 MeV. The present pulse forming network allows electron pulse widths between 200 ns and 2 μs but can be upgraded to allow pulse widths as long as 18 μs. At the waveguide's optimum energy of 25 MeV, the instantaneous current can be as high as 120 mA. The electron pulses can be supplied as a single shot or repeated at a rate up to 120 Hz [B8].

Similarly to proton radiography, magnetic focusing elements and lenses are positioned to focus the beam and obtain angular acceptance and resolution to radiograph objects. Radiographic contrast is established through collimation of electrons.

The low energy and small rest mass of the electrons results in this radiography system being very sensitive to thin objects. At 30 MeV the beam–object interactions are dominated by multiple Coulomb scattering. Figure B-3 shows approximate transmission plotted as a function of radiation lengths for 5, 10, 20 and 30 mrad collimation angles.

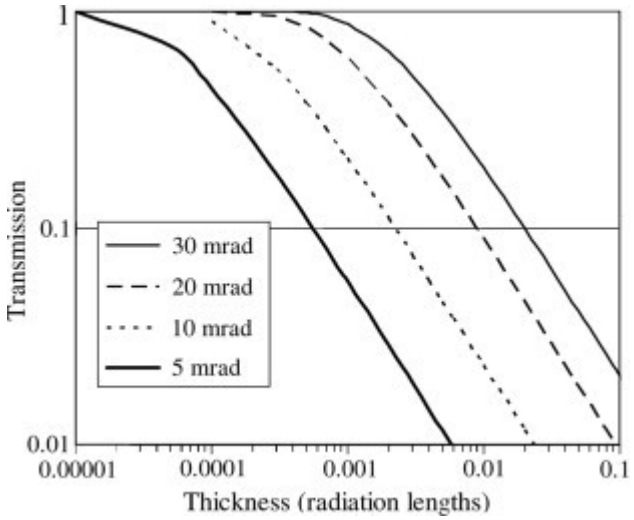

Figure B-3. Transmission versus thickness in units of radiation length with a 5, 10, 20 and 30 mrad collimator [B8].

Detailed measurements of resolution were collected by studying the step in transmission across the edge of a steel cylinder with a diameter of 2.5 cm. Radiographs of this horizontal and vertical edge are shown in Figure B-4.

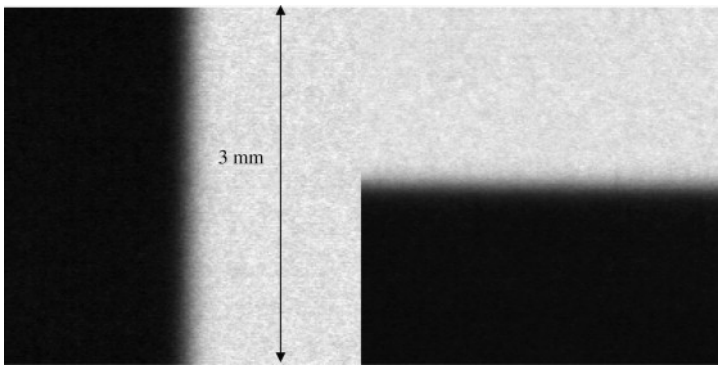

Figure B-4. Vertical edge transition used to measure horizontal resolution (left). The same edge transition rotated horizontally to measure vertical resolution (right) [B8].

A radiograph of a tungsten filament from a small light bulb is shown in Figure B-5. The diameter of the wire which forms the tungsten filament is 0.025 mm and the areal density is about 50 mg/cm^2. The large contrast seen in this radiograph shows that the sensitivity of the system to thin objects is well matched to the position resolution of the system. The significant contrast shown in this radiograph demonstrates the extreme sensitivity of this radiographic technique to thin objects with low areal densities.

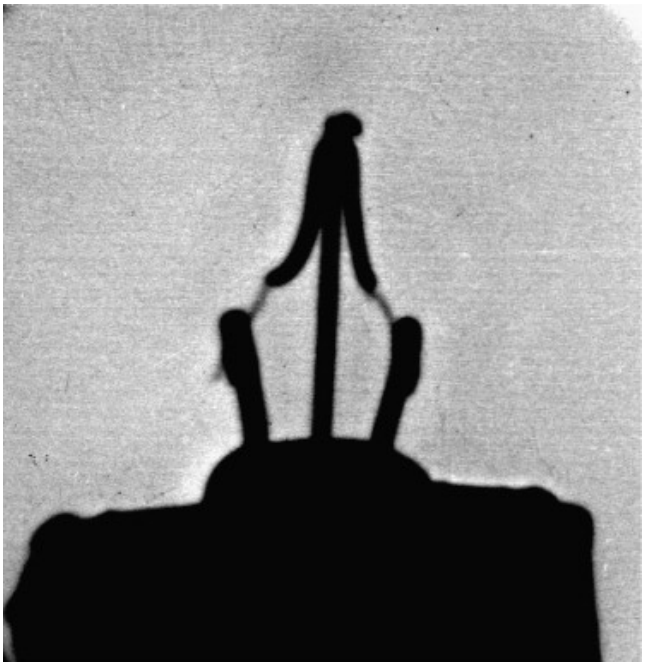

Figure B-5. Radiograph of a tungsten filament from a small light bulb [B8].

B.6. Dual-Axis Radiographic Hydrodynamic Test Facility

Dual-Axis Radiographic Hydrodynamic Test Facility (DARHT) was commissioned with the goal to maintain and verify the aging U.S nuclear stockpile in the absence of underground nuclear testing. A key to this capability is evaluation of the primaries of U.S. nuclear weapons through non-nuclear hydrodynamic testing, or "hydrotesting". These tests utilize very powerful X-ray sources to radiograph a full-scale, non-nuclear mock-up of a nuclear weapon primary during the late stages of the implosion, returning data on shapes, densities, and edge locations [B11].

The hydrotests experiments begin with two long electron accelerators arranged in an "L" shape. Magnetic fields are created which focus and steer a stream of electrons down its length. Significant electrical energy is added along the way. When these high-speed electrons, combined with the electrical energy, hit tungsten targets at the end of each leg of the "L" they are converted to X-rays intersecting at a firing point. This intense X-ray burst allows scientists to create dual-angle digital images and subsequently 3D models of mock nuclear devices as they implode [B12]. DAHRT has the capability to provide two kilo-ampere-class perpendicular beams of electrons in a 1 mm spot. The first axis delivers a single 60 ns bunches of 18 MeV electrons to a tungsten target, while the second axis delivers four bunches of 17 MeV electrons of variable length over a period of 1.8 μs [B13]. This radiographic facility is extremely useful in providing dual-axis multi-time radiography to support the US Stockpile Stewardship Program [B14].

APPENDIX C. RADIATION MEASUREMENTS AND RADIOGRAPHY APPLIED TO SPENT FUEL DRY STORAGE CASKS

This section reviews the published literature of radiography applied to spent fuel dry storage casks. This application is very similar to radiography for microreactors because there is central nuclear fuel surrounded by significant shielding. Thus the performance described here is a reasonable estimate of the performance applied to microreactors.

C.1. Fingerprint Method

In this method, researchers at Lawrence Livermore National Laboratory (LLNL) examined gamma and neutron radiation emission from six different types of dry cask storage containers containing spent nuclear fuel (SNF) [C1] . Each dry cask was unique with different amounts of shielding and construction materials. The fuel each cask contained was also unique with different types, burnup and cooling time. The objective was to produce a unique radiation based signature which acts as a 'fingerprint' of the fuel to identify if it was missing.

C.1.1. Detectors

Three detectors were used including a gamma ray imager, thermal neutron imager and germanium spectrometer. Both imagers employed a coded aperture imaging technique that relied on a shadow mask placed between the radiation source and a position-sensitive detector to encode the image spatially on the detector.

The gamma ray imager used a 12-cm diameter, 1-cm thick CsI disk mounted on a Hamamatsu R3292 position-sensitive-photomultiplier tube (PSPMT) [C1]. It is a prototype developed for arms-control applications and was optimized for low energy gammas with an upper energy threshold of 636 keV. This upper threshold was too low to image the gamma radiation escaping from the dry cask, causing unsatisfactory results.

The thermal neutron imager is a He-3 gas filled proportional counter with a crossed-wire and a 20-cm x 1-cm sensitive area. The detector was enclosed in a Cd lined box for thermal neutron absorption and was coupled with a coded-aperture mask.

The gamma-ray spectrometer is a high purity germanium (HPGe) detector with 39% relative efficiency. It was collimated with a bismuth annulus restricting its field of view to 10 degrees. An HPGe detector is not an imager but does have high gamma energy resolution which allows the identification of individual gamma rays. For this system, the dead time was kept below 26%.

C.1.2. Results and Discussion

Of the six casks available for measurements, the Westinghouse MC-10 cask present at the end of the pad was the most extensively measured due to ease of measurements as there were no spatial concerns, and the least background from neighboring casks.

Most of the gamma radiation that was measured had scattered in the shielding and had lost much of the original information it carries as it is emitted from the nuclear fuel, causing the resulting image to be unclear. The research concluded that a gamma imager with a larger surface area that is more sensitive to higher energy unscattered gammas should be developed to produce useful images.

Most of the neutron radiation was similarly scattered which created poor images that lacked any details of the dry cask. However, evidence suggests that significant fluences of higher-energy, unscattered neutrons exit the casks. Images obtained with instruments sensitive to this radiation may provide the requisite clarity to allow fingerprinting to succeed. Such devices are currently under development.

C.2. Cosmic Ray Muon Radiography

There have been multiple studies of cosmic ray muon radiography for nuclear waste in dry casks [C2-C6]. The method uses cosmic ray muons which are produced by interactions of protons and nuclei from space with atoms in the upper atmosphere. Collisions of these primary cosmic rays with atmospheric gas produce showers of pions, many of which decay to muons. These muons are highly energetic and highly penetrating. The incoming and outgoing muon trajectories are measured with two identical drift tube tracking detectors, which are placed on opposite sides of a dry cask. Muons passing through the tubes ionize the gas, and the resulting electrons drift towards the anode wire where they are multiplied through an avalanche process in the high electric field near the surface of the wire, producing a measureable signal. The muons incident on the top detector provide a starting position and direction. They then traverse the item through a series of multiple Coulomb scattering events. This phenomenon is when muons are deflected and slow down when they interact with material with a high atomic number or high Z. As negatively-charged muons pass through a volume, they interact with the negatively-charged electrons in the material and are deflected. After scattering on high Z material and changing their direction, muons are then detected by the lower detector, giving a final position and direction. The angles of deflection can be analyzed to gather information about the density of the item being measured [C7]. When multiple events are reconstructed, a density map can be obtained. The analysis of all this information combined can be used to produce images of the high Z material within the item of interest.

The muon radiography measurements typically take on the order of a week. The technique performs best if the detectors are directly above and below the item, but diagonal angles can also be used at the expense of longer measurement times. Also, more complicated geometries including replacing diverted assemblies with dummies and partially filed assemblies are not yet tested.

The technique discussed here is Cosmic Ray Muon Imaging of Spent Nuclear Fuel in Dry Storage Casks by J. Durham et. Al from Los Alamos National Laboratory [C2]. In this paper, a different method was developed to measure muons where measurements of the multiple scattering angle of individual muons passing through an object are used to create tomographic images of the object's interior structure.

C.2.1. Detectors

In this method, incoming and outgoing muon trajectories are measured with two identical drift tube tracking detectors that are placed on opposite sides of a dry cask. Each drift tube is made of aluminum with a length of 1.2 m and 5.08 cm diameter. It is filled with 1 bar of a 47.5% Ar, 42.5% CF_4, 7.5% C_2H_6, 2.5% He gas mixture. In the center of the tube, the anode wire is made of 30 micron diameter gold-plated tungsten. The principle of detection is similar to gas detectors where the muons passing through the tubes ionize the gas, and the resulting electrons drift towards the wire where they are multiplied through an avalanche process in the high electric field near the

surface of the wire, producing a measureable signal. The final detector consists of six double layers that are stacked with orientations alternating by 90 degrees in order to provide directional sensitivity.

A Westinghouse MC-10 spent fuel cask with partial fuel loading was imaged, Figure C-1. Two identical muon tracking detectors were placed on opposite sides of the cask in order to record the incoming and outgoing tracks of muons. One detector is elevated to take advantage of the higher muon flux at smaller zenith angles.

Figure C-1. Muon detectors around the MC-10 cask [C2].

There was concern that background from Compton scattered electrons would cause spurious pulses and affect the image reconstruction. This concern was mitigated by adding a trigger in the data acquisition system that required coincidence in neighboring tubes within 600 ns. Requiring coincidence reduced the counting rate by 50%. In the approximately 200 hour measurement, 1.62 x 10^5 muon tracks were recorded.

C.2.2. Results and Discussion

Measurement and simulation of the cask radiography is shown in Figure C-2 (a). The dashed lines show the approximate boundaries of columns in the fuel basket. While the general trend of the measurement and simulation are similar, the data was scaled by a factor of 1.2 to normalize the simulated count rate. This difference was likely observed due to differences in the muon momentum spectrum used in the simulation and the actual muon momentum that is present in measurements. Additionally, there are artifacts observed due to imprecise alignment of the detectors causing large offsets and biased aerial densities.

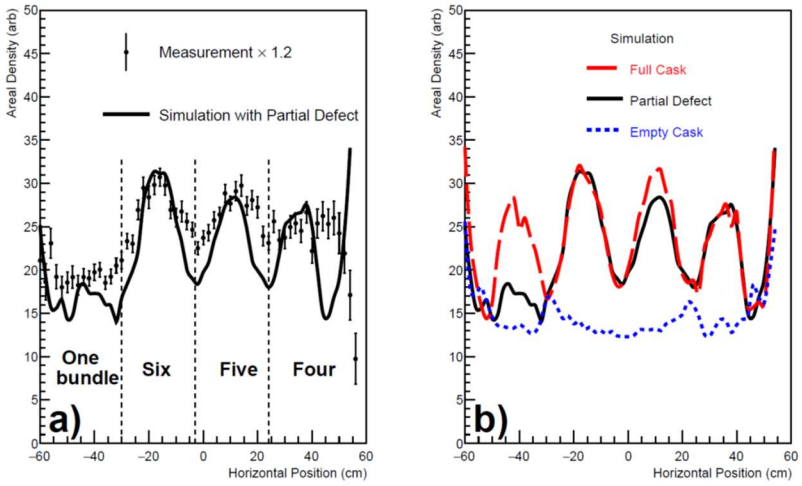

Figure C-2. Measured areal density through the cask (a), compared to a GEANT4 simulation of a cask with the same partial defect in loading. (b) Simulations of a completely full and empty cask [C2].

C.3. Passive Gamma Emission Tomography (PGET)

PGET measures the gamma emissions from spent fuel in a bare spent fuel assembly, creating a tomographic reconstruction of the structure of the fuel. The fuel does not have shielding so measurement of gamma rays that have not scattered is feasible. Adding significant shielding would make this technique difficult or impossible.

C.3.1. Detectors

The PGET instrument is made up of two banks of 87 CZT gamma ray detectors mounted on a plate behind a tungsten collimator inside a water-tight enclosure. Each plate rotates 360 degrees to measure gamma emissions around the entire fuel assembly. The CZT detector dimensions are 2 mm x 4.8 mm x 4.8 mm. The tungsten linear collimator slits are 10 cm deep, 1.5 mm wide, and taper from 70 mm tall at the front to 5 mm at the back. Figure C-3 shows a schematic of the instrument. For each measured data projection, each CZT detector records the number of counts above 4 user-determined gamma-ray energy thresholds. The thresholds are selected to enhance the contribution of ^{137}Cs and ^{154}Eu in each window.

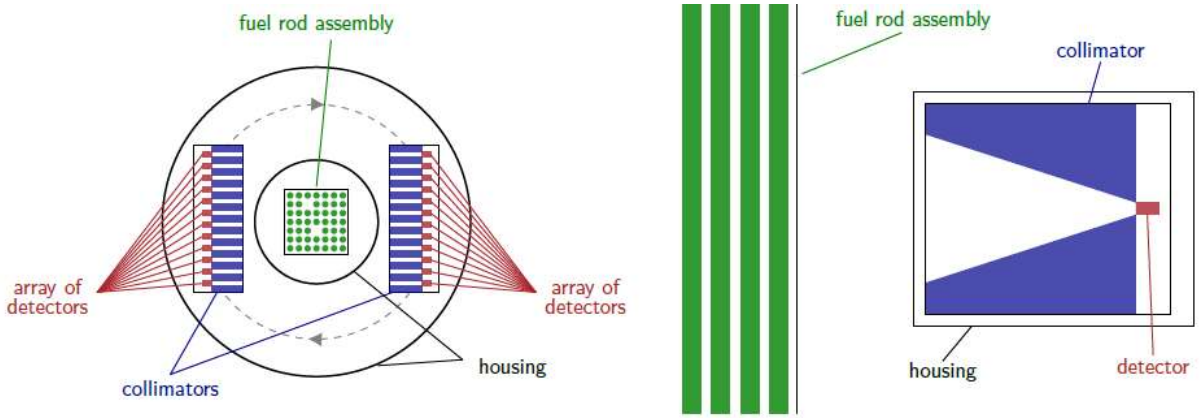

(a) Overhead view (b) Vertical cross section

Figure C-3. Simplified schematics of the PGET instrument. (a) Two detector banks on opposite sides of an SFA being measured. (b) Collimator slit profile and the location of the detectors with respect to the fuel rods [C7].

C.3.2. Methodology

Both the location of gamma emission and the location of gamma attenuation must be solved for because they both affect the measured count rates. The image reconstruction algorithm simultaneously solves for both. The algorithm bounds the range of activity and attenuation to assist in developing the solution, Figure C-4.

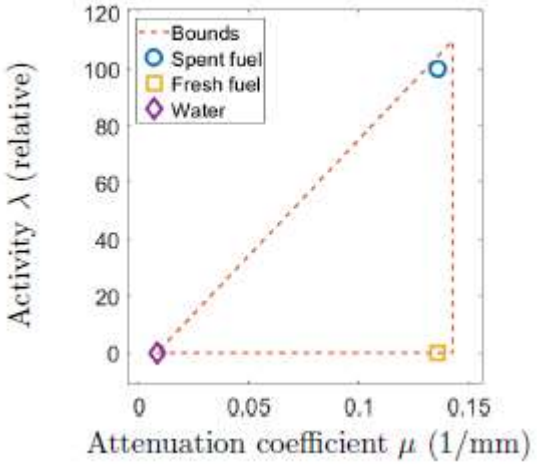

Figure C-4. Example of the bounds for the activity values and attenuation coefficients for 661 keV gamma rays used in the minimization process. The values inside the triangle are allowed [C8].

To estimate the activity and attenuation bounds and to build the matrices R_λ and R_μ for the geometry, rod locations and diameters are needed. The technique uses a filtered back projection (FBP) reconstruction method and then using the known grid and rod dimensions for that type of assembly. "In practice, the bounds for attenuation coefficients are estimated by considering the measurement energy window and the materials assumed to be imaged. Once the attenuation coefficients for water and rods are estimated, and locations and diameters for the rods are computed from having identified the assembly type, the upper bound for activity values is estimated by simulating a sinogram using rods with some uniform activity value *a*. The upper bound for activity values is then set so that the ratio of *a* and the maximum value of the simulated sinogram is the same as the ratio of the upper bound and the maximum value of the data sonogram" [C8]. The minimization problem is solved using a Levenberg-Marquardt type of algorithm.

C.3.3. Results and Discussion

In all of the paper's results, missing rods are clearly visible in the reconstructions and correctly classified by the algorithm. The central water channel is also classified as missing in both cases, Figure C-5.

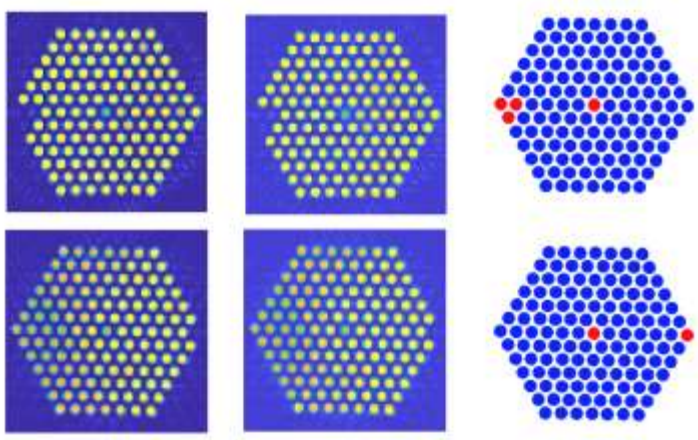

Figure C-5. Activity (left column) and attenuation (middle column) reconstructions and classification into missing (red) and present (blue) rods (right column) for two VVER-440 assemblies. Assembly #1 in the top row has three missing rods, a central water channel and 5 burnable absorber rods near the corners. Assembly #2 in the bottom row has one missing rod and a central water channel [C8].

C.4. Compton Dry Cask Imaging System

This method uses gamma ray imaging to identify diversions of spent fuel [C10]. ^{60}Co from neutron activation of stainless steel components of the fuel bundle, and ^{137}Cs which is a fission product, emit gamma rays that can be detected through the shielding of the dry cask. A removed fuel bundle will result in a lower count rate than expected.

C.4.1. Detectors

A tungsten collimated high purity germanium detector was placed on the outside of the dry cask lid above the known position of spent fuel assemblies. An x-y positioner ensured the detector is above the specific assembly, Figure C-6.

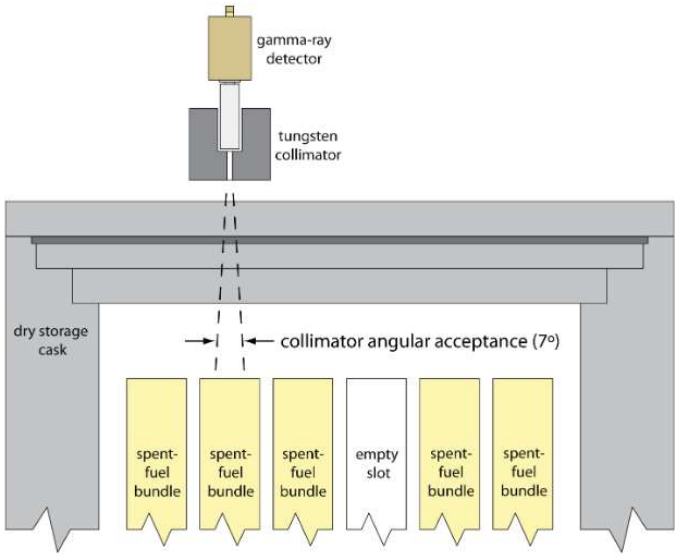

Figure C-6. A cutaway representation of the detector and collimator assembly, showing the limited angle through which gamma rays may pass [C10].

C.4.2. Methodology

When the detector is placed above a location that is filled, the unscattered gamma radiation reaches the detector and registers counts in spectral peaks. However, when positioned in an empty slot, a majority of the gammas have undergone Compton scattering and the energies are too low to register at the peak. The ratio of peak to Compton continuum counts is observed for every assembly position above the dry cask. The ratio of peak to Compton-continuum counts is high above full slots and low above empty slots.

C.4.3. Results and Discussion

In MCNP simulations the method was successful. However, in measurements, the system was unable to detect fission-product or activation gamma rays through the ballistic shield on top of the TN-24 cask. During the overnight automated runs, data was collected for 3,000 seconds on 18 full fuel bundles. The data collected from all 18 fuel bundles were added together to determine whether a longer count time would produce prominent photopeaks. The count time was equivalent to a 15 hour measurement and is shown in Figure C-7 below. In this "15-hour" spectrum, the Co-60, Cs-134, & Cs-137 peaks are still not identifiable. The gamma ray photopeaks seen in the recorded spectra could be attributed to either neutron interactions in the tungsten shielding or the germanium crystal of the detector

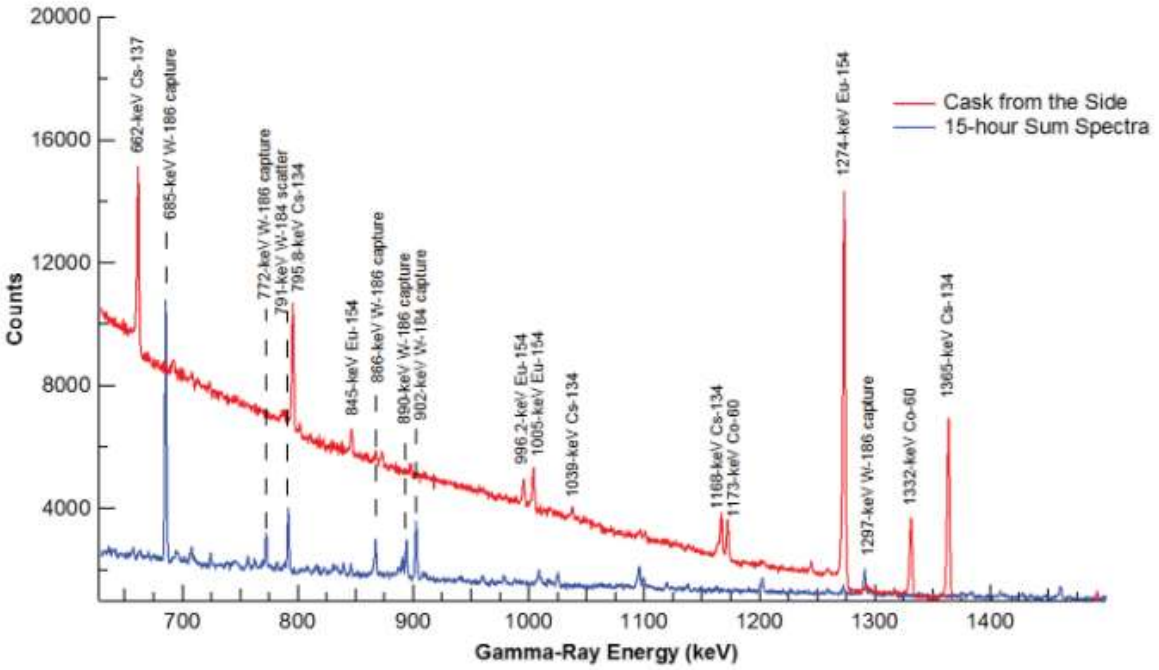

Figure C-7. Comparison of the 15-hour sum spectra and the 1-hour spectrum taken from the side of the cask. The spectral lines from the fission product dominate the side scan but are not present in the spectra from above, even after 15 hours [C10].

C.5. Neutron Fingerprinting of Dry Casks

C.5.1. Detectors and Methodology

In this computational study researchers from LANL evaluated the feasibility of neutron spectroscopy for safeguards of spent nuclear fuel in dry cask storage. Dry casks and their contents were modeled using the NGSI Spent Fuel Library, ORIGEN-S, and MCNP [24].

In the simulations 100 ^{4}He detectors were placed in a ring outside the cask at a specified height. The neutrons are detected by the scattering of fast neutrons on the helium gas. The scattering transfers a fraction of their kinetic energy to the ^{4}He nucleus dependent on the scattering angle. The ^{4}He recoil nucleus obtains a large kinetic energy and leaves the electrons behind. The recoiled alpha particle interactions with other helium atoms through excitation or ionization. Scintillation light is then emitted during the de-excitation which can be detected [24].

The neutron count rates form a signature or fingerprint of the dry cask. Diverted assemblies on the outside of the fuel are easily detected. Central assemblies are shielded by the other assemblies so the detection sensitivity is greatly reduced and identifying their diversion is challenging. The simulation is shown in Figure C-8.

In order to quantify the differences, a fingerprint value (FPV) was calculated. The FPV for each location is the individual neutron count rate divided by the average of all counts. The FPVs form a unique signature of the cask at the time of measurement. Because the rates are divided by the average of all counts, it normalizes away count rate changes due to fission product decay over time. Future measurements are compared to the initial measurement for each FPV and if it agrees within 4% it is accepted. If there are more than 8 rejected points, the fingerprint was considered to not match.

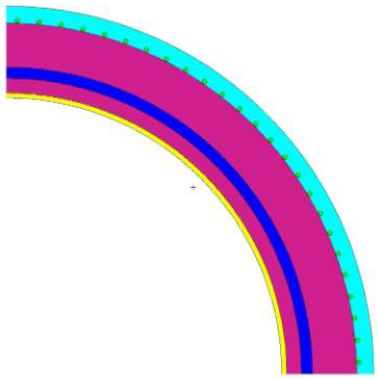

Figure C-8. Quarter view of modelled cask where circles represent the detectors [24].

C.5.2. Results and Discussion

Two simulated measurements were performed, one of the initial cask and another of the cask at a later time after radioactive decay. In the later simulation one fuel assembly was changed to represent diverted fuel. The simulation assumed a count time of 3 hours. The result in Figure C-9 demonstrates the method's sensitivity, and the test was successful because the location of the

different assembly was correctly identified and the FPVs matched where the assemblies were intact. There were multiple tests performed [24] that resulted in successful comparisons of fingerprints.

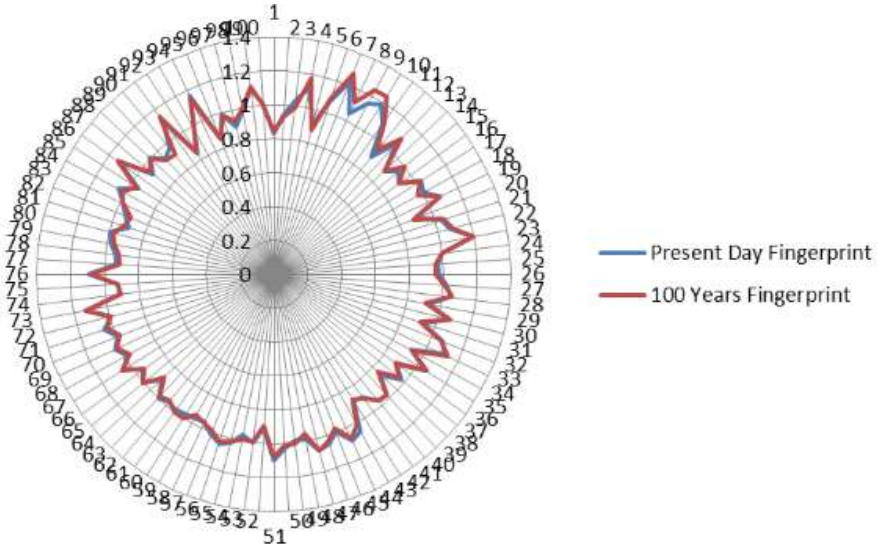

Figure C-9. Comparison of two similar fingerprints [24].

A rigorous feasibility study of the proposed method was completed and the results were promising enough to encourage continued research, starting with the creation of a more realistic simulation model. Additional future work includes the effect of multiple casks in close proximity and understanding the effect of detector placement.

C.6. Dual Slab Verification Detector

The Dual Slab Verification detector (DSVD) was built by Los Alamos National Laboratory in collaboration with the International Atomic Energy Agency as part of the dry storage safeguards system for spent fuel from the BN-350 fast reactor. The assemblies of the BN-350 reactor are hexagonal and contain uranium oxide rods and each dry cask contained between four to eight assemblies [C11,41].

C.6.1. Detectors

The DSVD consists of two rows of ten ^{3}He tubes, 4 atm pressure, 2.54 cm diameter, 61 cm long, encased in polyethylene slabs separated by a sheet of 1.5mm thick cadmium. The inner row of ^{3}He detectors was sensitive to neutrons emitted from the dry cask while the outer row simultaneously measured the background count rate from the neighboring casks. Preliminary experiments demonstrated that the total uncertainty with verifying the neutron emission characteristics of a dry storage cask is approximately ± 3% [C11,C12]. Past measurements are compared with current measurements to determine if a diversion has occurred. This method is viable, however it cannot be done independently without previous measurements.

C.6.2. Methodology

The front row of ^{3}He counters is designed to be sensitive to the neutron flux from the cask on interest, while the back row of counters are sensitive to the background neutrons from the neighboring casks.

This arrangement allows for a method for suppressing background neutrons and determining the neutron flux emitted. The measured neutron flux (φ_f) is given by

$$\varphi_f = \frac{C_f - R_f C_b}{\varepsilon_{ff} - R_f \varepsilon_{bf}}$$

where C_f and C_b are the measured count rates in the front and back slabs, respectively, ε_{ff} and ε_{bf} are the detection efficiencies of the front and back slabs, respectively, for neutrons from the front direction, and R_f is given by

$$R_f = \frac{\varepsilon_{fb}}{\varepsilon_{bb}}$$

C.6.3. Results and Discussion

DSVD verification measurements were performed in Aqtau, Kazakhstan during two separate spent fuel measurement campaigns that were several months apart.

From Figure C-10, reasonable agreement exists between the measured and simulated data during the first campaign. Both the measured and simulated count rates were normalized relative to the average measured count rate for that particular slab detector and spent fuel cask that was measured. However, several discrepancies were observed during this campaign and there is ongoing work to reduced and understand them.

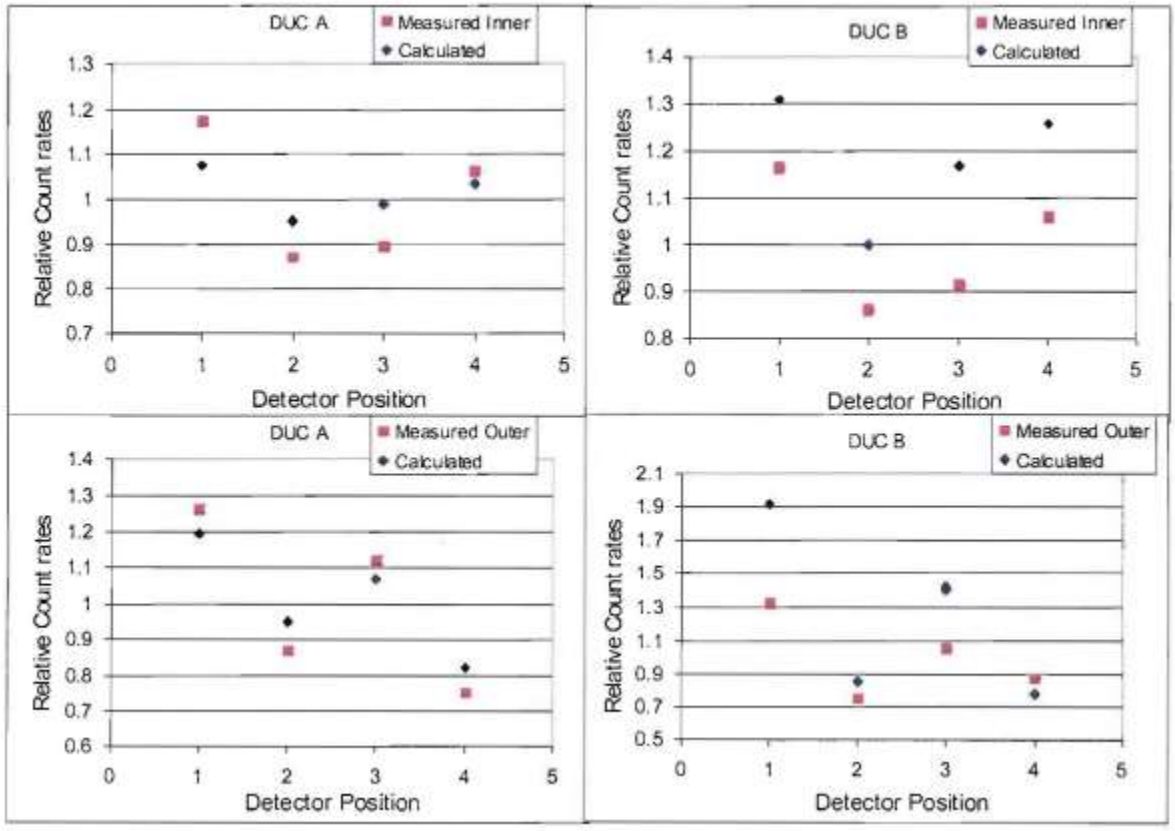

Figure C-10. Comparison between the measured relative count rates in the inner (top row) and outer (bottom row) slab detectors for two spent fuel casks labeled DUC A (left column) and DUC B (right column) and the simulated relative count rates. Both rates were normalized relative to the average measured count rate for a particular slab detector and spent fuel cask [C13].

In Figure C-11, there is good agreement in measured and simulated count rates for both slabs for the first 5 canisters that were placed in the cask. The first 5 canisters that were placed in the cask were placed in positions that were furthest away from the DSVD location. The next two canisters were placed in the positions that were closest to the DSVD, while the last canister was placed in the center of the cask. Work is currently ongoing to understand the large discrepancies.

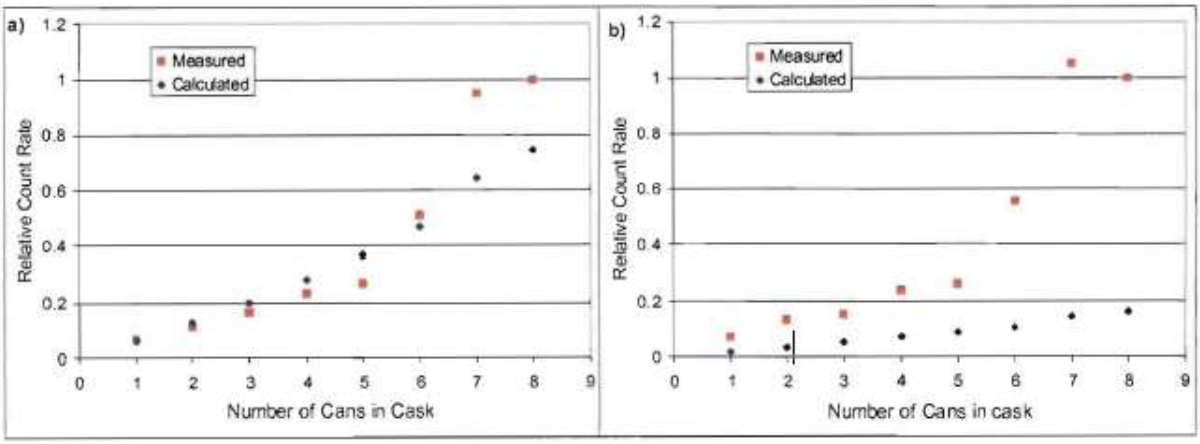

Figure C-11. Measured (red squares) and simulated (blue diamonds) count rates in the a) inner slab and b) outer slab as a function of the number of canisters that had been loaded into an empty cask. The count rates are relative to the measured count rates in the inner and outer slab, respectively, with all 8 canisters in the cask.

C.7. High Energy X-ray CT Simulation Study

In 2016, researchers at Missouri University of Science & Technology performed a simulation study of radiographing a dry cask using X-ray computed tomography. This technique is especially challenging due to the large amount of shielding which blocks most of the X-rays.

C.7.1. Detectors and Methodology

The equipment consisted of a high energy X-ray source, a set of scintillation based detectors, a post object collimator, and a data acquisition system. The X-ray source generated 4 MeV X-rays. The detector array moves 360 degrees around the cask while the source is projected in a fan beam. The source to detector (SDD) and source to object (SOD) distances are labelled in Figure C-12. The detector was modeled as an ideal detector with a pixel size of 1-mm which results in a spatial resolution of 0.6-mm at the isocenter if sufficient views per rotation are obtained. Spatial resolution of the CT scan is largely limited by the number of views per rotation. To achieve a submillimeter

spatial resolution, the number of views per rotation should be greater than 7160 (i.e., πD=7160 where D=2280 mm). A single scan can take as long as an hour [C14].

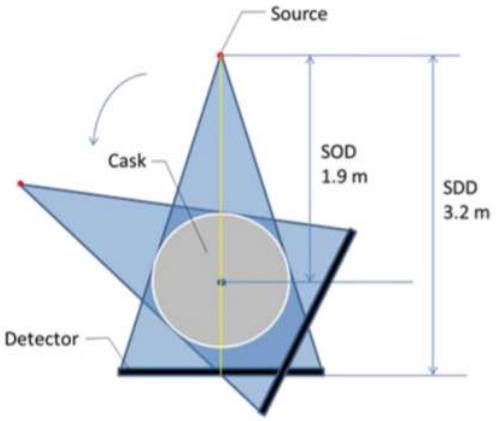

Figure C-12. Schematic plot of the X-ray tomographic simulation of an ideal case [C14].

In order to reduce the number of views per rotation without resolution degradation, region-of-interest (ROI) scans and iterative reconstruction algorithms were coupled. A smaller field of view (FOV) can be scanned instead of the entire cask as shown in Figure C-13. Alternatively, if the measurement time is held constant, a smaller FOV scan allows a smaller detector size and X-ray beam fan angle.

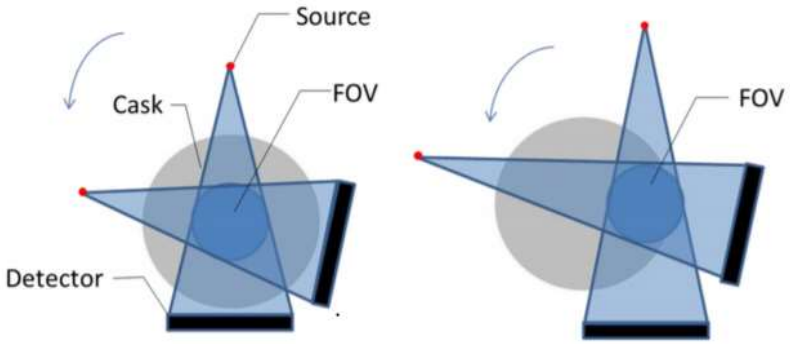

Figure C-13. Proposed scan schemes with smaller FOV: (1) the ROI is located at the center of the cask (left); (2) the ROI is located near the boundary of the cask (right) [C14].

C.7.2. Results and Discussion

The initial simulations ignored scatter and statistical noise. A total of 1000 views was used to image the cask at 0.36 degrees per view. A filtered-back-projection (FBP) reconstruction of a cross-section view of a TN-24 metal cask, with 24 pressurized water reactor (PWR) spent fuel assembles, is shown in Figure C-14. These simulations resulted in successful imaging of the cask contents. The artifacts were attributed to the low number of views and can be improved by increasing the number of views.

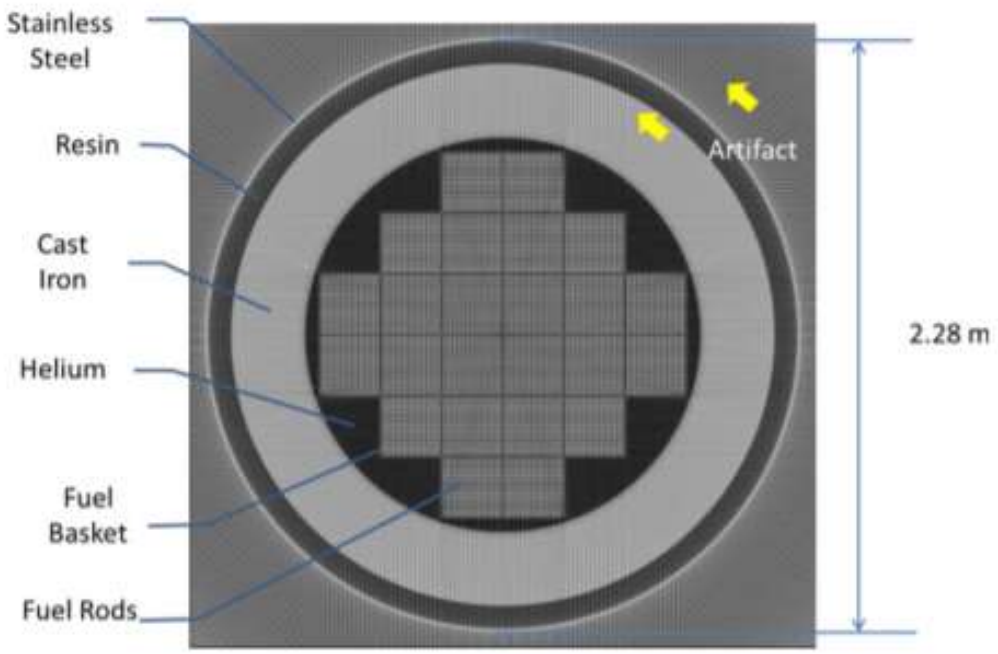

Figure C-14. Tomographic reconstructed cross-section view of a TN-24 metal cask. The simulation is performed with 1000 views and a 4 MeV X-ray beam.

Future scans included testing resolution for specific ROIs vs. the entire cask and imaging fuel rod damage. In all cases, the resulting images were successful in identifying the contents of the cask with few artifacts. One potential problem associate with this technique is the unprecedented long data collection time.

C.8. Neutron Remote Monitoring System (RMS) for Dry Casks

C.8.1. Detectors

Researchers at Texas A&M University devised two approaches for remotely monitoring dry casks using thermal neutron emissions from spent nuclear fuel. The approaches could be used together or separately to identify missing assemblies. The first design is an internal RMS that is deployed inside the dry cask before it is sealed, utilizing the concept of safeguards-by-design. The second design is an external RMS that can be placed outside a dry cask after it has been sealed. Both methods allow for Continuity of Knowledge on the contents of the dry cask and should be sensitive to potential diversions of SNF assemblies.

The internal RMS consists of two fission chambers to detect thermal neutrons. The fission chambers are surrounded with polyethylene and a natural cadmium sheet underneath the polyethylene as shown in Figure C-15 [C15].

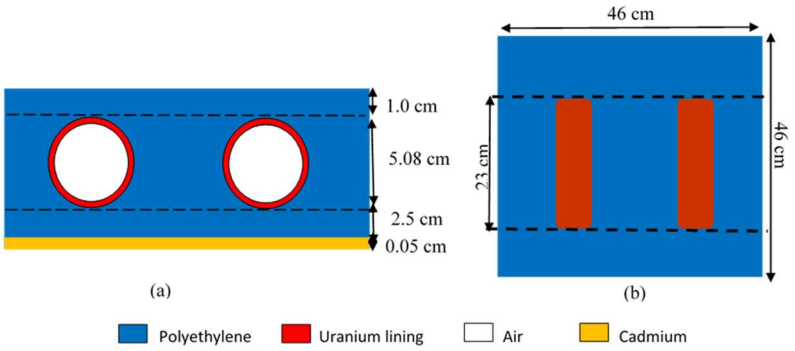

Figure C-15. Internal RMS with fission chambers denoted by uranium lining and air, polyethylene and cadmium shown in (a) front view and (b) top view [C15].

The second approach is the external RMS that uses an array of micro-structured semiconductor neutron detectors (MSNDs). The MSNDs represent a compact, low-cost, high efficiency means of solid-state thermal neutron detection. These detectors claim to have thermal neutron efficiencies as high as 30% for single sided and over 65% for double sided configurations [C16]. The external RMS comprised of eight MSNDs in a 4 x 2 array enveloped in an optimized amount of polyethylene, placed on the outer lid of a dry cask, Figure C-16.

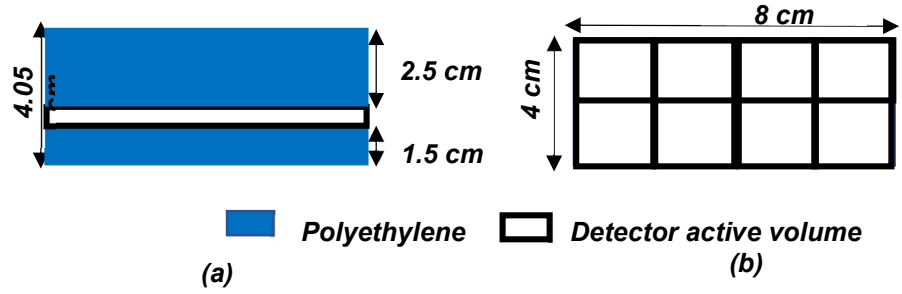

Figure C-16. External RMS with MSND detectors shown in (a) front view and (b) top view [C17].

C.8.2. Methodology and Results

The eight scenarios that were simulated consisted of single and double assembly diversions which were substituted with fresh fuel dummies. Gross thermal neutron counts were obtained by the detectors. Alarm thresholds and an acceptable false alarm probability were chosen. The corresponding non-detection probability was calculated for a specified measurement time [C18]. All non-detection probabilities were below 20% per IAEA guidance.

In addition to the eight diversion scenarios for homogenous loading, three heterogeneous spent fuel loading patterns were simulated for both RMS designs. In all cases, both RMS designs quickly identified the presence of a dummy assembly replacing a spent fuel assembly [C15,C17,C18]. For

both RMS designs, the non-detection probabilities proved to be under 20% for all assembly diversion cases.

Small scale experiments were performed as proof of concept measurements for the internal RMS using ^{252}Cf sources as surrogates for SNF. The sources were reflected with either graphite or polyethylene to diffuse the thermal neutron flux to more closely represent a volumetric source. The flux distribution then mimics the geometry of a spent fuel assembly. The analysis of these experiments concluded that neutron source diversion mimicking the diversion of SNF was detectable. Hence, this technology is shown to be accurate, cost effective and a viable alternative to in-person inspections.

REFERENCES

[1] PART 74—MATERIAL CONTROL AND ACCOUNTING OF SPECIAL NUCLEAR MATERIAL, NRC Web. (n.d.). https://www.nrc.gov/reading-rm/doc-collections/cfr/part074/full-text.html#part074-0031 (accessed December 14, 2020).

[2] Westinghouse, eVinci Micro-Reactor, https://www.westinghousenuclear.com/new-plants/evinci-micro-reactor, accessed 2021

[3] Urenco, Separative Work Unit calculator, https://www.urenco.com/swu-calculator, accessed 2021

[4] D. Bernauer, Radiant Nuclear Company Overview, presented to the August 2020 Microreactor Program virtual workshop, (2020)

[5] D. Proctor, Former SpaceX Engineers Tout New Microreactor, Power Magazine, September (2020)

[6] C. Filippone, K. A. Jordan, The Holos Reactor, engrXiv preprints (2017)

[7] Design and technology features of the U-battery, IAEA technical meeting on microreactors, April (2021)

[8] U-Battery Consortium, UBattery A Future Energy Solution brochure, (2021)

[9] World Nuclear News, U-Battery SMR moves to next stage of Canadian Assessment, (2019)

[10] Y. Arafat, J. Van Wyk, eVinci Micro Reactor, Nuclear Plant Journal, March-April (2019)

[11] Ultra Safe Nuclear Corporation, MMR Energy System, https://usnc.com/mmr-energy-system/, accessed 2021

[12] F. Reitsma, Design and technology features of the MMR and its deployment pathway, IAEA technical meeting on microreactors, April (2021)

[13] C.Cochran, Microreactors: Technology readiness and market opportunities, American Nuclear Society 2021 Annual Meeting, (2021)

[14] Nuclear Newswire, Oklo awarded $2 million to commercialize advanced fuel recycling, (2021)

[15] MIT News, Zach Winn, Commercializing next-generation nuclear energy technology, https://news.mit.edu/2020/oklo-nuclear-energy-1113, (2020)

[16] PART 52—LICENSES, CERTIFICATIONS, AND APPROVALS FOR NUCLEAR POWER PLANTS, NRC Web. (n.d.). https://nrc.gov/reading-rm/doc-collections/cfr/part052/full-text.html (accessed December 15, 2020).

[17] J.W. Sterbentz, J.E. Werner, M.G. McKellar, A.J. Hummel, J.C. Kennedy, R.N. Wright, J.M. Biersdorf, Special Purpose Nuclear Reactor (5 MW) for Reliable Power at Remote Sites Assessment Report, 2017. https://doi.org/10.2172/1410224.

[18] C.J. Werner, et al., "MCNP6.2 Release Notes", Los Alamos National Laboratory, report LA-UR-18-20808 (2018).

[19] Integrated Security and Detection Systems, Decis. Sci. (n.d.). https://decisionsciences.com/ (accessed December 15, 2020).

[20] C.L. Morris, J. Bacon, Y. Ban, K. Borozdin, J.M. Fabritius, M. Izumi, H. Miyadera, S. Mizokami, Y. Otsuka, J. Perry, J. Ramsey, Y. Sano, T. Sugita, D. Yamada, N. Yoshida, K. Yoshioka, Analysis of muon radiography of the Toshiba nuclear critical assembly reactor, Appl. Phys. Lett. 104 (2014) 024110. https://doi.org/10.1063/1.4862475.

[21] J. Perry, ADVANCED APPLICATIONS OF COSMIC-RAY MUON RADIOGRAPHY, Nucl. Eng. ETDs. (2013). https://digitalrepository.unm.edu/ne_etds/4.

[22] J.M. Durham, D. Poulson, J. Bacon, D.L. Chichester, E. Guardincerri, C.L. Morris, K. Plaud-Ramos, W. Schwendiman, J.D. Tolman, P. Winston, Verification of Spent Nuclear Fuel in Sealed Dry Storage Casks via Measurements of Cosmic-Ray Muon Scattering, Phys. Rev. Appl. 9 (2018) 044013. https://doi.org/10.1103/PhysRevApplied.9.044013.

[23] D. Poulson, J. Bacon, M. Durham, E. Guardincerri, C.L. Morris, H.R. Trellue, Application of muon tomography to fuel cask monitoring, Philos. Trans. R. Soc. Math. Phys. Eng. Sci. 377 (2019) 20180052. https://doi.org/10.1098/rsta.2018.0052.

[24] E. Rauch, S. Demuth, Developing a Method for Unique Identification of Used Fuel Storage Casks Using Neutrons, 2014. https://doi.org/10.2172/1159064.

[25] Z. Liu et al., Neutron Tomography of Spent Fuel Casks, Journal of Signal Processing Systems (2021)

[26] A.S. Tremsin, S.C. Vogel, M. Mocko, M.A.M. Bourke, V. Yuan, R.O. Nelson, D.W. Brown, W.B. Feller, Non-destructive studies of fuel pellets by neutron resonance absorption radiography and thermal neutron radiography, J. Nucl. Mater. 440 (2013) 633–646. https://doi.org/10.1016/j.jnucmat.2013.06.007.

[27] P. Vontobel, E.H. Lehmann, R. Hassanein, G. Frei, Neutron tomography: Method and applications, Phys. B Condens. Matter. 385–386 (2006) 475–480. https://doi.org/10.1016/j.physb.2006.05.252.

[28] Force Sensors, Force Transducers and Load Cells [N], HBM. (2020). https://www.hbm.com/en/0249/force-sensors-and-force-transducers/ (accessed December 14, 2020).

[29] H.O. Menlove, Description and Performance Characteristics for the Neutron Coincidence collar for the Verification of Reactor Fuel Assemblies, LA-8939-MS (1981)

[30] H.O. Menlove et al., Neutron Collar Calibration and Evaluation for Assay of LWR Fuel Assemblies Containing Burnable Neutron Absorbers, LA-11965-MS (1990)

[31] Photonis boron-lined proportional counters. https://www.photonis.com/products/boron-lined-proportional-counters

[32] A.P. Simpson et al., Improved Neutron Counting Methods for Characterization of Gaseous Diffusion Plant Process Equipment, ESARDA NDA Working Group (2015)

[33] R. Weinmann-Smith et al., Measurement and simulation of cosmic ray effects on neutron multiplicity counting, Nuclear Instruments and Methods in Physics Research A 814 (2016) 50-55

[B1] C. for D. and R. Health, What is Computed Tomography?, FDA. (2020). https://www.fda.gov/radiation-emitting-products/medical-X-ray-imaging/what-computed-tomography (accessed November 23, 2020).

[B2] Essentials of Radiology - 3rd Edition, (n.d.). https://www.elsevier.com/books/essentials-of-radiology/mettler/978-1-4557-4225-7 (accessed November 24, 2020).

[B3] A review of imaging techniques in scientific research/clinical diagnosis, MOJ Anat. Physiol. Volume 6 (2019). https://doi.org/10.15406/mojap.2019.06.00269.

[B4] L.M. Biga, S. Dawson, A. Harwell, R. Hopkins, J. Kaufmann, M. LeMaster, P. Matern, K. Morrison-Graham, D. Quick, J. Runyeon, 1.5 Medical Imaging, in: Anat. Physiol., OpenStax/Oregon State University, 2019. https://open.oregonstate.education/aandp/chapter/1-5-medical-imaging/ (accessed November 24, 2020).

[B5] L.O. Lerman, M. Rodriguez-Porcel, J. Carlos Romero, The development of X-ray imaging to study renal function, Kidney Int. 55 (1999) 400–416. https://doi.org/10.1046/j.1523-1755.1999.00301.x.

[B6] S.M. Kelkar, Using X-ray Imaging Techniques to Determine Density of Foods, (n.d.) 214.

[B7] Archiving, Chapter 2: Medical Image Data Characteristics - Society for Imaging Informatics in Medicine, SIIM.Org. (n.d.). https://siim.org/page/archiving_chapter2 (accessed November 24, 2020).

[B8] Electron radiography, Nucl. Instrum. Methods Phys. Res. Sect. B Beam Interact. Mater. At. 261 (2007) 382–386. https://doi.org/10.1016/j.nimb.2007.04.127.

[B9] C.L. Morris, E.N. Brown, C. Agee, T. Bernert, M.A.M. Bourke, M.W. Burkett, W.T. Buttler, D.D. Byler, C.F. Chen, A.J. Clarke, New developments in proton radiography at the Los Alamos Neutron Science Center (LANSCE), Exp. Mech. 56 (2016) 111–120.

[B10] K.E. Kippen, R.D. Fulton, E. Brown, W.T. Buttler, A.J. Clarke, K.K. Kwiatkowski, F.G. Mariam, F.E. Merrill, C. Morris, R.T. Olson, M. Zellner, AOT & LANSCE Focus: Proton Radiography Facility, 2013. https://doi.org/10.2172/1083846.

[B11] M.J. Burns, B.E. Carlsten, T.J.T. Kwan, D.C. Moir, D.S. Prono, S.A. Watson, E.L. Burgess, H.L. Rutkowski, G.J. Caporaso, Y.- Chen, S. Sampayan, G. Westenskow, DAHRT accelerators update and plans for initial operation, in: Proc. 1999 Part. Accel. Conf. Cat No99CH36366, 1999: pp. 617–621 vol.1. https://doi.org/10.1109/PAC.1999.795776.

[B12] Meet a Machine: DARHT uses accelerators and X-rays to validate nuclear simulations, Energy.Gov. (n.d.). https://www.energy.gov/nnsa/articles/meet-machine-darht-uses-accelerators-and-X-rays-validate-nuclear (accessed December 3, 2020).

[B13] C.L. Morris, N.S.P. King, K. Kwiatkowski, F.G. Mariam, F.E. Merrill, A. Saunders, Charged particle radiography, Rep. Prog. Phys. 76 (2013) 046301. https://doi.org/10.1088/0034-4885/76/4/046301.

[B14] R.D. Scarpetti, S. Nath, J. Barraza, C.A. Ekdahl, E. Jacquez, B.T. McCuistian, K. Nielsen, M. Schulze, J. Seitz, G.J. Caporaso, Y.-J. Chen, G. Logan, F. Bieniosek, Status of the darht 2nd axis accelerator at the Los Alamos national laboratory, in: 2007 IEEE Part. Accel. Conf. PAC, IEEE, Albuquerque, NM, 2007: pp. 831–835. https://doi.org/10.1109/PAC.2007.4441094.

[C1] K.P. Ziock, P. Vanier, L. Forman, G. Caffrey, J. Wharton, A. Lebrun, The Feasibility of Cask "Fingerprinting" as a Spent-Fuel, Dry-Storage Cask Safeguards Technique, UNT Digit. Libr. (2005). https://doi.org/10.2172/881660.

[C2] J.M. Durham, E. Guardincerri, C.L. Morris, D. Poulson, J.D. Bacon, D. Chichester, J. Fabritius, S. Fellows, K. Plaud, D. Morley, P. Winston, Cosmic Ray Muon Imaging of Spent Nuclear Fuel in Dry Storage Casks, (n.d.) 14.

[C3] M. Österlund, J. Blomgren, J. Donnard, A. Flodin, J. Gustafsson, M. Hayashi, P. Mermod, L. Nilsson, S. Pomp, L. Wallin, A. Öhrn, A. Prokofiev, TOMOGRAPHY OF CANISTERS FOR SPENT NUCLEAR FUEL, (2006).

[C4] G. Jonkmans, V.N.P. Anghel, C. Jewett, M. Thompson, Nuclear waste imaging and spent fuel verification by muon tomography, Ann. Nucl. Energy. 53 (2013) 267–273. https://doi.org/10.1016/j.anucene.2012.09.011.

[C5] F. Ambrosino, L. Bonechi, L. Cimmino, R. D\textquotesingleAlessandro, D.G. Ireland, R. Kaiser, D.F. Mahon, N. Mori, P. Noli, G. Saracino, C. Shearer, L. Viliani, G. Yang, Assessing the feasibility of interrogating nuclear waste storage silos using cosmic-ray muons, J. Instrum. 10 (2015) T06005–T06005. https://doi.org/10.1088/1748-0221/10/06/T06005.

[C6] A. Clarkson, D.J. Hamilton, M. Hoek, D.G. Ireland, J.R. Johnstone, R. Kaiser, T. Keri, S. Lumsden, D.F. Mahon, B. McKinnon, M. Murray, S. Nutbeam-Tuffs, C. Shearer, C. Staines, G. Yang, C. Zimmerman, The design and performance of a scintillating-fibre tracker for the cosmic-ray muon tomography of legacy nuclear waste containers, Nucl. Instrum. Methods Phys. Res. Sect. Accel. Spectrometers Detect. Assoc. Equip. 745 (2014) 138–149. https://doi.org/10.1016/j.nima.2014.01.062.

[C7] R. Backholm, T.A. Bubba, C. Bélanger-Champagne, T. Helin, P. Dendooven, S. Siltanen, Simultaneous Reconstruction of Emission and Attenuation in Passive Gamma Emission Tomography of Spent Nuclear Fuel, ArXiv190503849 Phys. (2019). http://arxiv.org/abs/1905.03849 (accessed November 11, 2020).

[C8] R. Virta, R. Backholm, T.A. Bubba, T. Helin, M. Moring, S. Siltanen, P. Dendooven, T. Honkamaa, Fuel rod classification from Passive Gamma Emission Tomography (PGET) of spent nuclear fuel assemblies, ArXiv200911617 Phys. (2020). http://arxiv.org/abs/2009.11617 (accessed November 11, 2020).

[C10] G. Caffrey, Compton Dry-Cask Imaging System, Idaho National Lab. (INL), Idaho Falls, ID (United States), 2011. https://www.osti.gov/sciencecinema/biblio/1046053 (accessed November 11, 2020).

[C11] P.A. Santi, Testing of the Dual Slab Verification Detector for Attended Measurements of the BN-350 Dry Storage Casks., (n.d.) 13.

[C12] P. Santi, M. Browne, R. Williams, R. Parker, Testing of the dual slab verification detector for attended measurements of the BN350 dry storage casks, (2020).

[C13] M.C. Browne, C.R. Freeman, R.F. Parker, R.B. Williams, Title: Initial Measurements of BN-350 Spent Fuel in Dry Storage Casks using the Dual Slab Verification Detector, (n.d.) 11.

[C14] A simulation study of the spent nuclear fuel cask condition evaluation using high energy X-ray computed tomography | Elsevier Enhanced Reader, (n.d.). https://doi.org/10.1016/j.ndteint.2016.02.008.

[C15] A. Sagadevan, Safeguards Approach for Spent Nuclear Fuel in Dry Cask Storage using Remote Monitoring Systems, PhD dissertation, Texas AM University, n.d.

https://nsspi.tamu.edu/safeguards-approach-for-spent-nuclear-fuel-in-dry-cask-storage-using-remote-monitoring-systems-74694/ (accessed September 28, 2020).

[C16] R.G. Fronk, S.L. Bellinger, L.C. Henson, D.E. Huddleston, T.R. Ochs, M.A. Reichenberger, C.J. Rietcheck, C.T. Smith, T.J. Sobering, J.K. Shultis, D.S. McGregor, Advancements in microstructured semiconductor neutron detector (MSND)-based instruments, in: 2015 IEEE Nucl. Sci. Symp. Med. Imaging Conf. NSSMIC, 2015: pp. 1–5. https://doi.org/10.1109/NSSMIC.2015.7581971.

[C17] Athena Sagadevan, Sunil Chirayath (Texas A&M), Safeguards Approaches for Remote Monitoring System of Spent Nuclear Fuel Dry Cask Storage, in: n.d.

[C18] A. Sagadevan, S. Chirayath, Information driven safeguards approach for remote monitoring system of dry cask storage, Nucl. Instrum. Methods Phys. Res. Sect. Accel. Spectrometers Detect. Assoc. Equip. 954 (2020) 161737. https://doi.org/10.1016/j.nima.2018.12.052.